Showcasing research from Prof. Yuichi Negishi's laboratory, Tokyo University of Science, Japan.

The structure and application portfolio of intricately architected silver cluster-assembled materials

This review provides a succinct overview of the trajectory of silver cluster-assembled materials research, with crucial insights into atomic-level structural correlations with the phenomena at the nanoscale and discussion of the gaps and opportunities that are still open in addition to charting a roadmap for future research directions.

As featured in:

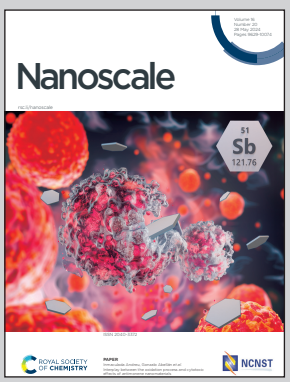

See Saikat Das, Yuichi Negishi *et al.*, *Nanoscale*, 2024, **16**, 9642.

ROYAL SOCIETY OF CHEMISTRY

rsc.li/nanoscale

Registered charity number: 207890

Nanoscale

REVIEW

View Article Online
View Journal | View Issue

Cite this: *Nanoscale*, 2024, **16**, 9642

The structure and application portfolio of intricately architected silver cluster-assembled materials

Riki Nakatani, [a] Saikat Das *[b] and Yuichi Negishi *[a,b]

Received 2nd March 2024,
Accepted 7th April 2024

DOI: 10.1039/d4nr00905c

rsc.li/nanoscale

Silver Cluster-Assembled Materials (SCAMs) represent a new frontier of crystalline extended solids hallmarked by their customizable structures, commendable stabilities, and unique physical/chemical properties. Since their discovery in 2017, the diversity of organic linkers has endowed SCAMs with ingenious architectures and the application scenario has expanded beyond photoluminescence sensing to environmental sustainability and biomedical applications. It is critically important to chronicle these recent key advances and review the progress of SCAMs that can enable translating the material discoveries into real implementation. Herein, we provide a succinct overview of the trajectory of SCAM research, with crucial insights into atomic-level structural correlations with the phenomena at the nanoscale and discuss the gaps and opportunities that are still open in addition to charting a roadmap for future research directions.

1 Introduction

Nanoclusters are aggregates of metal atoms and their diameters are mostly 1–3 nm; they have been drawing attention as nanomaterials since the late 20th century because they demonstrate characteristics different from those of single metal atoms or bulk.[1,2] Looking more closely at the structure of a nanocluster, the structure consists of a core composed of metal atoms and a shell formed of ligands around the core. The core can not only be composed of a single metal species, but also of multiple metal species, which can have a great impact on stability, optoelectronic properties, catalytic performance and so on.[3,4] On the other hand, the shell has been of great importance because it not only contributes to the stabilization of the nanocluster structure, but also prevents aggregation between clusters and determines their properties and structures.[5] However, nanoclusters have several shortcomings: they are notorious for their low yields, and the purity of the nanoclusters obtained is not high, making their purification and characterization considerably more difficult than for simple metal complexes.[6] Therefore, the separation of clusters has also been the subject of substantial research in the field of nanomaterials.[7] In addition to separation, there have been intensive studies on how to extend the use of clusters. Nanoclusters are largely used in a diverse array of applications, including photochemistry, electrochemistry, catalysis, sensing and others.[8–11] Among them, silver has outstanding physical properties and is cheaper and more plentiful as a resource than gold, which is also a kind of precious metal.[12] Numerous attempts have been made to synthesize silver nanoclusters with unique optical absorption properties.[13–16] However, silver has a critical drawback of being easily oxidized by exposure to air and light that has greatly limited its range of applications compared to other precious metals.[17]

In light to the foregoing, cutting-edge materials that can solve the most important issue of stability of silver clusters are silver cluster-assembled materials (SCAMs). SCAMs are crystalline extended structures connecting silver cluster nodes and organic linkers through coordination bonds. $[(Ag_{12}(S^tBu)_8(CF_3COO)_4(bpy)_4)]_n$ (henceforth denoted as Ag_{12}bpy) SCAM was prepared by Zang *et al.* upon substituting 4,4′-bipyridine (bpy) for coordinated acetonitrile (CH_3CN) ligands of Ag_{12} nanoclusters.[18] Ag_{12}bpy showed stability far superior to that of discrete silver nanoclusters under many conditions, including prolonged exposure to air and light irradiation, and the luminescence quantum yield was dramatically improved. The organic linkers used for cross-linking not only stabilize the structure by linking clusters together, but also contribute to the SCAM properties.[19] The structure of SCAMs can also be modified by changing the shape of the linker to form unique structures. Thereafter, many SCAMs utilizing bidentate, tridentate, and tetradentate linkers other than bpy have been reported.[20–24] On the other hand, in terms of silver nanoclusters, which are the nodes of SCAMs, there have been reports of SCAMs constituted by nanoclusters of

[a]*Department of Applied Chemistry, Faculty of Science, Tokyo University of Science, Kagurazaka, Shinjuku-ku, Tokyo 162-8601, Japan. E-mail: negishi@rs.tus.ac.jp*
[b]*Research Institute for Science & Technology, Tokyo University of Science, Kagurazaka, Shinjuku-ku, Tokyo 162-8601, Japan. E-mail: saikatdas@rs.tus.ac.jp*

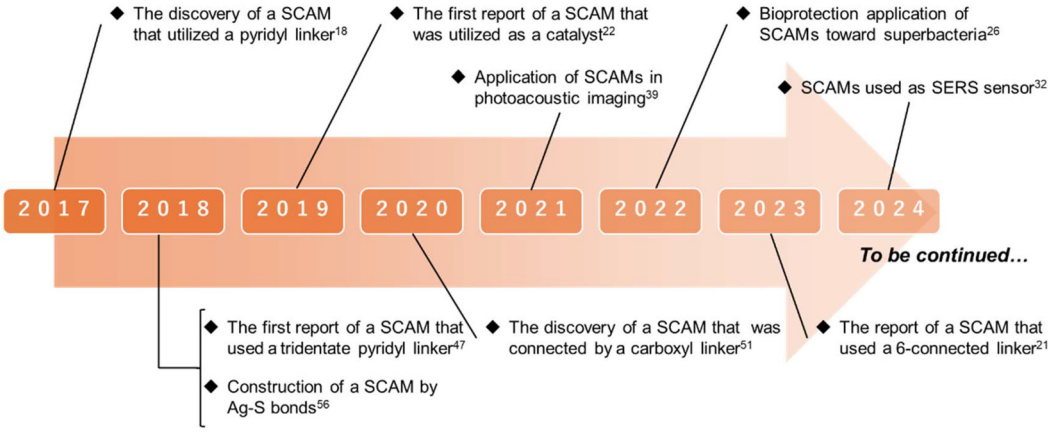

Fig. 1 Timeline charting the evolutionary pathway of SCAMs.

different numbers of silver atoms such as Ag_9, Ag_{10}, Ag_{27},[21,25,26] *etc.*, in addition to the more commonly known Ag_{12} cluster-based SCAMs. Hence, it can be said that SCAMs can not only resolve the stability problem of silver nanoclusters through metal–ligand coordination, but also display structural diversity. In addition to linking the silver cluster nodes *via* organic linkers, there have been instances of linking the silver cluster nodes without linker molecules to form one-dimensional (1D),[27,28] two-dimensional (2D)[28,29] and three-dimensional (3D) frameworks.[28–31]

In this review, we briefly describe the crystalline structures, synthetic procedures, and applicability of SCAMs, which, as mentioned before, exhibit wide structural, morphological and functional diversity. Notably, most SCAMs yet reported have been constructed from pyridyl linkers; however, there are a few reports on structures built from carboxyl and thiourea linkers.[20] From the viewpoint of synthetic procedures, it is difficult to predict the architectural complexity of the SCAM structures, as it may be possible to synthesize SCAMs by relatively facile routes such as the one-pot approach in which the organic linker is directly added to the solution of the metal precursor under stirring or the liquid–liquid diffusion method in which the reaction occurs at the interface between the inorganic and organic phases.[26,32] In terms of application, SCAMs have shown use for a myriad of applications. The primary ones are the applications associated with luminescence. Intriguingly, many applications utilizing this property revealed that the emission peaks of SCAMs are different from those of linkers.[21,33] In addition, there are also reports of SCAMs being used as sensors by harnessing the advantage of their structural stability as well as change in their luminescence behavior upon interaction of the analytes with the framework.[21,34] Benefitting from the extended network structures that promote access to active sites and substrate diffusion into the active site as well as cooperative functions of silver clusters and organic linkers, SCAMs have been used for catalytic and bioprotection applications.[19,22,26] The molecular-level designability, structural versatility and tunability of emission properties have enabled the emergence of SCAMs as optically active nanomaterials. Therefore, this article aims to provide a systematic overview of the unique structural and functional characteristics of SCAMs and their distinct features as an assembly relative to the building blocks from the perspective of systems chemistry and condensed matter chemistry, the correlation between structure and properties of these materials, and the attributes of individual structural components in the obtained networks and their interactions that add up to the sum total property of the entire framework *i.e.* how the extended frameworks in the condensed phase can not only inherit the properties from building blocks and local structures but also bring forth its uniqueness in achieving luminescence behavior and catalytic activity. Fig. 1 illustrates the milestones in SCAM research.

2 Structures of SCAMs

The structure of SCAMs is vast, and since the structures are dictated by multiple factors, including the structure of the linker, the number and position of sites that can form coordination bonds, the steric hindrance, and the number of silver atoms that make up the silver nanocluster, even a slight difference in the structure of the constituent units leads to a great diversity of SCAM structures. The structure of SCAMs can be deciphered by single-crystal X-ray diffraction (SC-XRD) analysis. In this section, we introduce the currently reported structures of SCAMs on the basis of the coordination number of the linker and the type of coordination bond.

2.1 SCAMs formed by Ag–N bonds

There are many structures of SCAMs with Ag–N bonds. Here we introduce some of them.

2.1.1 Bidentate linkers. The emergence of bidentate linkers in the construction of SCAMs marked a new chapter in the history of SCAMs. Ag_{12}bpy, synthesized by Zang *et al.* in 2017, generated colossal interest.[18] The core of silver nano-

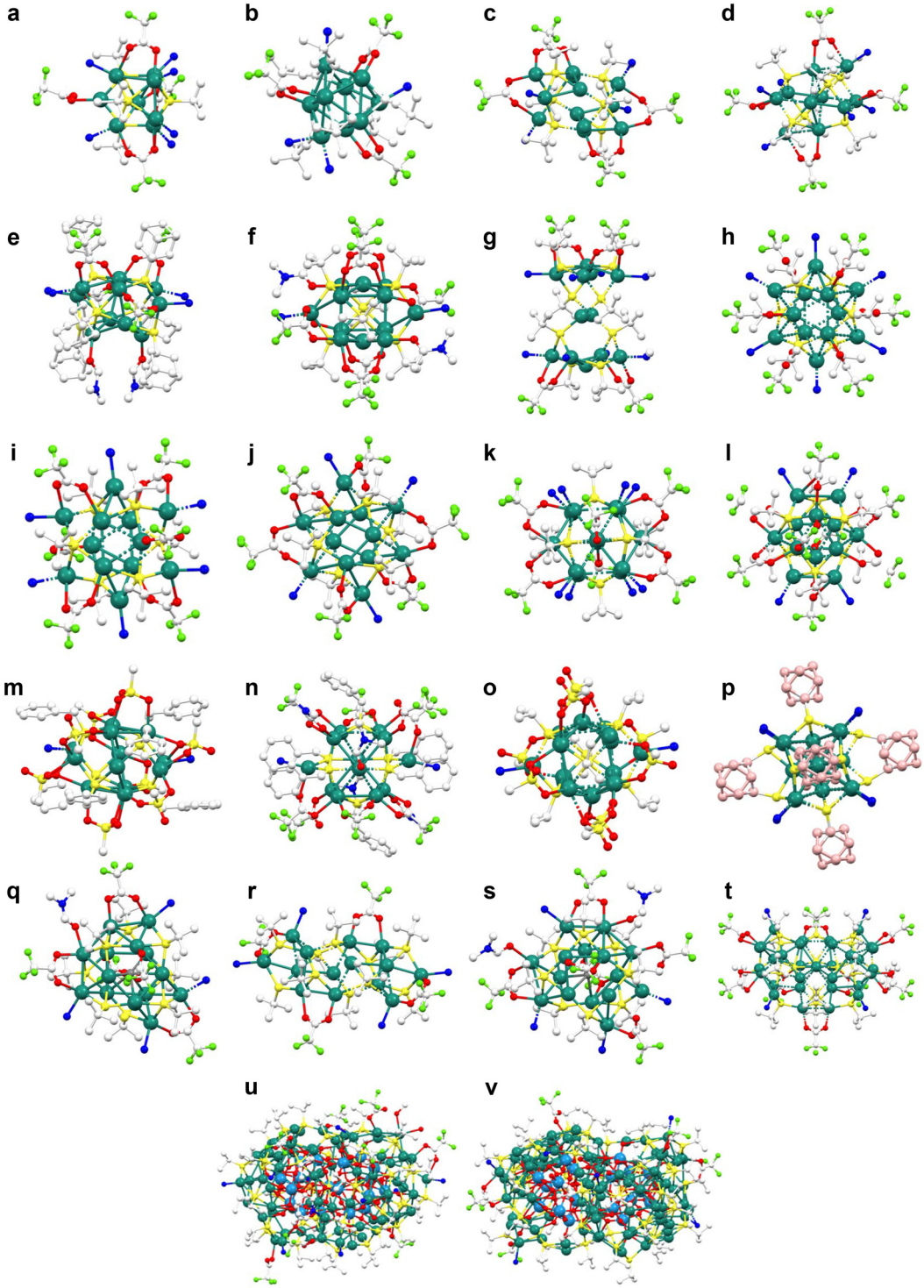

Fig. 2 Structural representation of each SCAM node. Ag_8, Ag_9, Ag_{10}, Ag_{11}, Ag_{12}, Ag_{14}, Ag_{15}, Ag_{27} and Ag_{72} are shown in (a), (b), (c) and (d), (e), (f)–(o), (p)–(r), (s), (t), and (u) and (v), respectively (green: Ag, yellow: S, white: C, blue: N, light green: F, red: O, pink: B, gray: Cl, orange: P, and light blue: W).

clusters in Ag_{12}bpy is $Ag_{12}S_8$, which is composed of Ag_5S_2–Ag_2S_4–Ag_5S_2 in a three-layer structure with a twisted conformation (Fig. 2g and 3a). The upper and lower layers of Ag_5S_2 have a square pyramidal arrangement, while the middle layer of Ag_2S_4 features a tetrahedral arrangement. Trifluoroacetic acid is coordinated to this core in such a way that each of the four molecules of trifluoroacetic acid is coordinated to two silver atoms. Since bpy is a bidentate ligand, the structure is one-dimensionally extended. The crystal system was found to be tetragonal with the space group of $I\bar{4}2m$. Thus, Ag_{12}bpy has

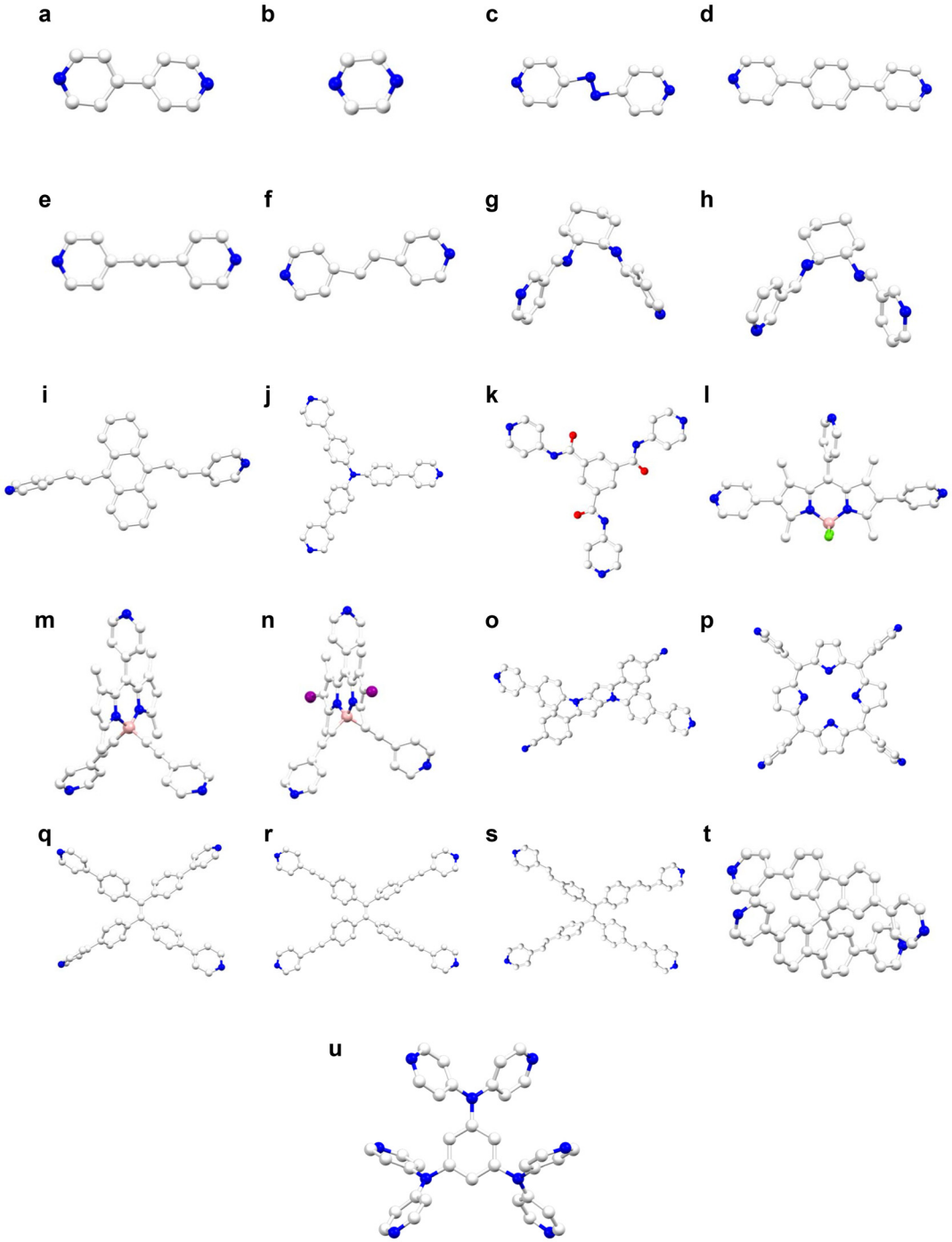

Fig. 3 (a)–(u) Structural representation of pyridyl linkers used in the construction of SCAMs (white: C, blue: N, red: O, pink: B, light green: F, and purple: I).

a 2D structure that extends into the *ab* plane (Fig. 5a). Besides, the layers of the SCAM are stacked in the *ABAB* fashion. The crystal structure of Ag_{12}bpy after 10 hours of exposure to 420 nm light, after adsorption experiments of oxygen, nitrogen, and ethanol gases, and after one year was evaluated using powder X-ray diffraction (PXRD) with no detectable peak changes, implying that the structure is extremely stable.

Zang *et al.* reported four new SCAMs, SCAM-1,2,3,4 (SCAM-1 = $\{[Ag_{14}(C_2B_{10}H_{10}S_2)_6(Pyrazine)_{6.5}(DMAc)(CH_3CN)_{0.5}]\cdot 2DMAc\}_n$, SCAM-2 = $\{[Ag_{14}(C_2B_{10}H_{10}S_2)_6(dpd)_2(CH_3CN)_4]\cdot DMAc\}_n$, SCAM-3 = $\{[Ag_{14}(C_2B_{10}H_{10}S_2)_6(bpy)_4]\}_n$, and SCAM-4 = $\{[Ag_{14}(C_2B_{10}H_{10}S_2)_6\ (dpbz)_4]\}_n$), in 2018.[35] In these syntheses, $[Ag_2(C_2B_{10}H_{10}S_2)\ (CH_3CN)_2]_n$ was used as a precursor. Focusing on the structure of each SCAM, each reported SCAM node is

composed of $Ag_{14}(C_2B_{10}H_{10}S_2)_6$ that consists of six protecting ligands located on the vertex of the octahedron. In these SCAMs, there are eight possible sites for linker coordination, which correspond to the apex of the cube (Fig. 2p). SCAM-1 comprises six and a half pyrazine (Fig. 3b), one DMAc, and half a CH_3CN molecules. However, due to the small size of the pyrazine molecules, they are sterically hindered and cannot form a higher dimensional structure, so only the diagonal pyrazines are coordinated to form a 1D structure that extends along the *c*-axis. In SCAM-2, four dipyridin-4-yl-diazene (Fig. 3c) and four CH_3CN are coordination bonded. Unlike the pyrazine used in SCAM-1, its large molecular size makes it suitable for cross-linking, and all four dipyridin-4-yl-diazene cross-link clusters together. As a result, SCAM-2 forms a 2D structure that extends over the *bc* plane. Regarding SCAM-3, some of the coordination sites are not solvent molecules as in SCAM-1 and 2, but all eight are composed of bpy (Fig. 3a), which is used for cross-linking. As a result, the secondary building unit (SBU) formed an octahedral structure, while SCAM-3 formed a structure extending to 3D space. SCAM-4 consists of a 1,4-bis(4-pyridyl) benzene linker (Fig. 3d), which has a longer molecular length than that of SCAM-3. Like SCAM-3, the SCAM-4 structure adopts a 3D structure with eight linkers attached to the node. This structure showed high stability owing to interpenetration, which was confirmed to be maintained even after nitrogen adsorption experiments. The structure was also highly stable at elevated temperatures up to *ca.* 220 °C, as corroborated by variable-temperature PXRD. In terms of crystal systems and space groups, SCAM-1 was trigonal and $P3_2$, SCAM-2 was monoclinic and $C2/m$, SCAM-3 was tetragonal and $P4/mnc$, and SCAM-4 was tetragonal and $P4_1/a$, respectively.

In the same year, Zang *et al.* reported that Ag_{12}bpy was converted to $[(Ag_{12}(S^tBu)_6(CF_3COO)_6(bpy)_3)]_n$ (Ag_{12}bpy-2) by adding Ag_{12}bpy to a mixture of DMAc and toluene, and conversely, Ag_{12}bpy-2 to a mixture of ethanol and CH_3CN.[36] First, a comparison in the core structure of the clusters showed that the Ag_{12} core in Ag_{12}bpy formed D_{2d} symmetry (Fig. 2g), while the Ag_{12} core in Ag_{12}bpy-2 underwent a symmetry change to C_{3v} (Fig. 2h). This change in the core structure was found to have caused a variety of structural changes, including dipole moments, the number of bonds between Ag atoms, and the strength of argentophilic interactions. It was also confirmed that the structure of SCAM changes depending on the type of solvent used in the synthesis. These changes were confirmed by SC-XRD, which showed that the crystal system was tetragonal in Ag_{12}bpy but changed to trigonal in Ag_{12}bpy-2, and that the space group changed from $I\bar{4}2m$ in Ag_{12}bpy to $P\bar{3}$ in Ag_{12}bpy-2.

A novel 1D SCAM $[Ag_{10}(S^tBu)_6(CF_3CF_2COO)_4(CH_3CN)_2(bpy)_2]_n$ (denoted as Ag_{10}bpy-CH_3CN) (Fig. 2c) was discovered by Zang *et al.*[34] This SCAM showcased an unique feature where the crystal structure changes to $[Ag_{10}(S^tBu)_6(CF_3CF_2COO)_4(bpy)_2]_n$ (Ag_{10}bpy) after removal of the coordinating CH_3CN molecules, and like Ag_{12}bpy described above, reversible transformation between Ag_{10}bpy and Ag_{10}bpy-CH_3CN. Both cluster nodes had $Ag_{10}S_6$ as the core and four $CF_3CF_2COO^-$ anions were used as anionic ligands, bridged by two bpy linkers (four bpy in total). The crystal system and space group of the SCAM were identified as triclinic and $P\bar{1}$, respectively.

In 2019, Zang *et al.* reported $[Ag_{12}(S^tBu)_6(CF_3COO)_6(bpa)_3(DMAc)_{12}]_n$ (Ag_{12}bpa) and $[Ag_{12}(S^tBu)_6(CF_3COO)_6(bpe)_3(DMAc)_{14.7}]_n$ (Ag_{12}bpe) with Ag_{12} cluster nodes bridged by 1,2-bis(4-pyridyl) ethane (bpa, Fig. 3e) and 1,2-bis(4-pyridyl) ethylene (bpe, Fig. 3f).[23] The nodes of these two SCAMs (Fig. 2h) have structural similarity with that of Ag_{12}bpy-2, and both the crystal system and space groups were trigonal and $P\bar{3}$. Immersion of both of them in CH_3CN entailed a phenomenal change in both: the structure of 2D Ag_{12}bpa was transformed into a 1D structure, Ag_{10}bpa (Fig. 2c). This change made the crystal system triclinic and the space group $P\bar{1}$. On the other hand, Ag_{12}bpe was converted to Ag_{12}bpe-1b, accompanied by minor distortion of the $Ag_{12}S_6$ node caused by the contact of Ag_{12}bpe with CH_3CN and changes in stacking patterns (Fig. 2i). The crystal system and space group of Ag_{12}bpe-1b also changed to monoclinic and $P2_1/c$, respectively. In addition, Ag_{12}bpe-1b could be irreversibly converted to Ag_{10}bpa by immersion in a CH_3CN solution of bpa. This study demonstrated that the structural conversion of SCAM depends on the flexibility of the linker used.

In the same year, Bakr and co-workers reported $[Ag_{15}Cl(S^tBu)_8(CF_3COO)_{5.67}(NO_3)_{0.33}(bpy)_2(DMF)_2]\cdot 4.3\text{-}(DMF)\cdot H_2O$ (hereinafter 1-D NCF) and $[Ag_{14}Cl(S^tBu)_8(CF_3COO)_5(bpy)_2(DMF)]\cdot 2(DMF)$ (hereinafter 2-D NCF), which contain Cl anions in the cluster.[37] The interesting aspect of this report was that the synthesis can be accomplished by adding bpy to the synthesis scheme of Ag_{16} nanoclusters using Cl anions as the template. 1-D NCF's Ag_{15} core structure was $Ag_{15}S_8Cl$, and the structure was asymmetric because one Ag atom is absent from the Ag_{16} nanocluster. Consequently, the number of Ag atoms bridged by six S atoms is four and the number of Ag atoms bridged by two S atoms is three. Among the six CF_3COO^- ions present as protective ligands around the core, four CF_3COO^- ions located equatorially form bonds to the two Ag atoms. The remaining two CF_3COO^- ions are located in the axial positions, one bridging to three Ag atoms and one bridging to two Ag atoms. Of the CF_3COO^- ions in the equatorial position, there is one with an occupancy of 0.67, and the remaining 0.33 is occupied by a NO_3 anion ligand believed to be appearing from the remaining silver nitrate in AgS^tBu. Out of 4 bpy linkers linking one Ag cluster with three adjacent Ag clusters, 2 bpy linkers link another two Ag clusters in one dimension and the remaining two bpy ligands form bridged structures with the third cluster (Fig. 2s). The crystal system of 1-D NCF was triclinic, and its space group was $P\bar{1}$. Next, looking at the structure of 2-D NCF, the node Ag_{14} nanocluster has a structure such that two Ag atoms are missing from the Ag_{16} nanocluster, and the core was $Ag_{14}S_8Cl$. 4 S atoms form coordination bonds with 4 different Ag atoms, and the remaining S atoms form coordination bonds with three Ag atoms. Out of the five CF_3COO^- ligands protecting the Ag_{14} core, all of the five CF_3COO^- ions are coordinated to two Ag

atoms, and only the CF_3COO^- ligand in the axial position showed different types of coordination modes. This is also like 1-D NCF, the Ag_{14} nanoclusters in 2-D NCF are bridged to three different nanoclusters by four bpy linkers (Fig. 2q). The crystal system and space group of this crystal structure were determined as triclinic and $P\bar{1}$, respectively. Thermogravimetric analysis (TGA) studies revealed that the thermal stability of the SCAMs increased with the complexity of the structures.

A study by Zang and colleagues presented the postsynthetic modification strategy of the parent SCAM utilizing the functional group of the linker.[38] First, an amine-substituted linker, 1,4-bis(pyrid-4-yl) benzenamine (NH_2-bpz), was used to prepare a SCAM named NH_2-Ag_{12}bpz. The amine group was then covalently bonded to methacrylic anhydride (MA) and polymerized by a photoinduced free radical reaction using butyl methacrylate (BMA) or triethylene glycol dimethacrylate (TEGDMA) as the acrylate monomer. In the SCAM membranes developed using varying polymerization ratios of BMA and TEGDMA, BMA enhanced the mechanical strength of the membranes while TEGDMA imparted the membranes with flexibility. The resulting structure with both coordination and covalent bonds is rewarding for higher structural complexity as well as synergistic effects.

In 2021, Mandal *et al.* reported a newly synthesized SCAM, $[Ag_{14}(S^tBu)_{10}(CF_3COO)_4(4,4'\text{-azopyridine})_2]$ (Ag_{14}CAM), with the $Ag_{14}S_{10}$ nanocluster core having a distorted polyhedral shape composed of eight square and eight triangular faces, and surrounded by ten S^tBu and four CF_3COO^- ligands (Fig. 2r).[39] Ag_{14}CAM adopted a 2D structure and had an *ABC* stacking pattern in the *ac* plane. Another intriguing feature of this study is that ethanol and acetonitrile were used as solvents in the synthesis of Ag_{14}CAM, but crystals with different shapes were obtained even when ethanol and chloroform were used. However, the latter SCAM was found to have the same crystalline structure as the former (crystal system: monoclinic, space group: *C*2/*c*), as evaluated by SC-XRD and PXRD analyses.

In the same year, Dong, Li and co-workers succeeded in synthesizing a novel SCAM by bringing further innovations to the linker.[40] Cucurbit[6]urils-*N*,*N*′-hexamethylene-bis(pyrazinylhexafluorophosphate) (BPHF@CB[6]), which was used as the linker of the reported SCAM, is a complex composed of CB and BPHF through host–guest interactions. The incorporation of CB into linear BPHF is known to exhibit unprecedented structural and chemical properties. The use of BPHF@CB[6] as a bidentate linker has led to the formation of three new SCAMs: $[Ag_{12}(SC_7H_7)_6(CH_3SO_3)_8(BPHF@CB[6])]_n$, $[Ag_{12}(SC_7H_7)_6(CF_3COO)_8(DMF)_3(CH_3OH)(BPHF@CB[6])]_n$, and $[Ag_{12}(^iPrS)_6(CH_3SO_3)_8(BPHF@CB[6])]_n$, hereinafter denoted as SCM 1, SCM 2, and SCM 3, respectively. The silver cluster core of SCM 1 is protected by a CH_3SO_3 anion ligand and SC_7H_7, and BPHF@CB[6] formed a 1D wave-like structure by forming Ag–N coordination bonds at two of the six Ag atoms in the asymmetric position of the intermediate layer (Fig. 2m). The crystal system of SCM 1 was ascertained as monoclinic, and the space group as *P*2/*c*. The CF_3COO^- ligands protecting the core of SCM 2 have two kinds of protecting patterns: two CF_3COO^- protect one Ag atom and six of them protect two Ag atoms. BPHF@CB[6] generated a linear 1D SCM 2 by forming two Ag–N coordination bonds with respect to the symmetric position of the intermediate layer in the cluster node (Fig. 2n). The crystal system of SCM 2 was characterized as monoclinic, as in SCM 1, but the space group was $P2_1/n$. Similar to SCM 1 and 2, SCM 3 also featured a 1D structure (Fig. 5b), with a BPHF@CB[6] linker bridging the clusters, each of the six $^iPrS^-$ ligands protecting four Ag atoms and eight $CH_3SO_3^-$ ligands protecting the cluster node (Fig. 2o). Unlike SCM 1 and SCM 2, the crystal system of SCM 3 was identified as triclinic and the space group was $P\bar{1}$.

A work introducing a new 1D SCAM $[Ag_{11}(AdmS)_6(CF_3COO)_4(apy)_2(DMF)_2][NO_3]$ (Ag_{11}CAM, AdmSH = adamantanethiol, apy = 4,4′-azopyridine) using the Ag_{11} cluster node was reported by Mandal *et al.*[41] The cluster core was composed of $Ag_{11}S_6$, surrounded by six $AdmS^-$ and four CF_3COO^- ligands. This is the first reported SCAM in which AdmS was utilized as a protective ligand. The clusters were bridged by two apy linkers, and there were four Ag–N coordination bonds per cluster (Fig. 2e). The Ag_{11}CAM stacked in the *ABA* pattern. NO_3^- ions were found to be accommodated as counter anions in the lattice spacing.

Another paper by Mandal *et al.* reported 1D $[Ag_2(PhPO_3H)_2(apy)_2]$ (apy = 4,4′-azopyridine) (hereinafter referred to as Ag_2apy), which did not use thiols as stabilizing ligands.[42] The two $PhPO_3H^-$ ligands form coordination bonds opposite to each other with both Ag atoms constituting the cluster nodes. The two apy linkers connecting the clusters are aligned parallel to each other at an average distance of 3.74 Å. The crystal system of the Ag_2apy SCAM was triclinic and the space group was $P\bar{1}$.

In 2021, Teo, Zheng and colleagues used a chiral Ag_{14} nanocluster as the node and two chiral bidentate linkers, (1*R*,2*R*, N^1E,N^2E)-N^1,N^2-bis(pyridine-3-ylmethylene)-cyclohexane-1,2-diamine (hereinafter LR) (Fig. 3g) and (1*S*,2*S*, N^1E,N^2E)-N^1,N^2-bis(pyridine-3-ylmethylene)-cyclohexane-1,2-diamine (hereafter LS) (Fig. 3h) to construct $[Ag_{14}(SPh(CF_3)_2)_{12}(PPh_3)_4(LR)_2]_n$ (denoted as Ag_{14}-LR) and $[Ag_{14}(SPh(CF_3)_2)_{12}(PPh_3)_4(LS)_2]_n$ (denoted as Ag_{14}-LS) enantiomeric SCAMs (Fig. 4a and b).[43] Ag_{14}-LR/LS adopted a 3D structure constructed by the replacement of four DMF molecules (originally coordinated to the nanoclusters) by linkers. Both crystal systems were hexagonal, and the space groups were $P6_122$ for Ag_{14}-LR and $P6_522$ for Ag_{14}-LS. The thermal durability of both SCAMs up to *ca.* 150 °C was validated by PXRD studies. It was also confirmed that the Ag_{14} nanoclusters building Ag_{14}-LR/LS were homochiral. In other words, the racemic Ag_{14} clusters were transformed into homochiral building units that led to the SCAMs. Moving further, the racemic form of the linker LR/LS (LRS) was used. The SCAM crystal structure obtained by using this racemic form contained *R*-Ag_{14} and *S*-Ag_{14} in a 1 : 1 ratio. Unlike Ag_{14}-LR/LS, the crystal system of Ag_{14}-LRS was orthorhombic and the space group was *Pnnn*.

In 2022, Sun and co-workers presented $\{[(PW_9O_{34})_2@Ag_{72}S(^iPrS)_{41}(CF_3COO)_8(bipy)_{5.5}(CH_3OH)(H_2O)]\cdot 3CF_3COO\}_n$ (hereinafter referred to as SD/Ag_{72}a) (bipy: 4,4′-bipyridine) and $\{[(PW_9O_{34})_2@Ag_{72}S(^iPrS)_{42}(CF_3COO)_7(\text{pi-bipy})_{4.5}(CH_3OH)]\cdot$

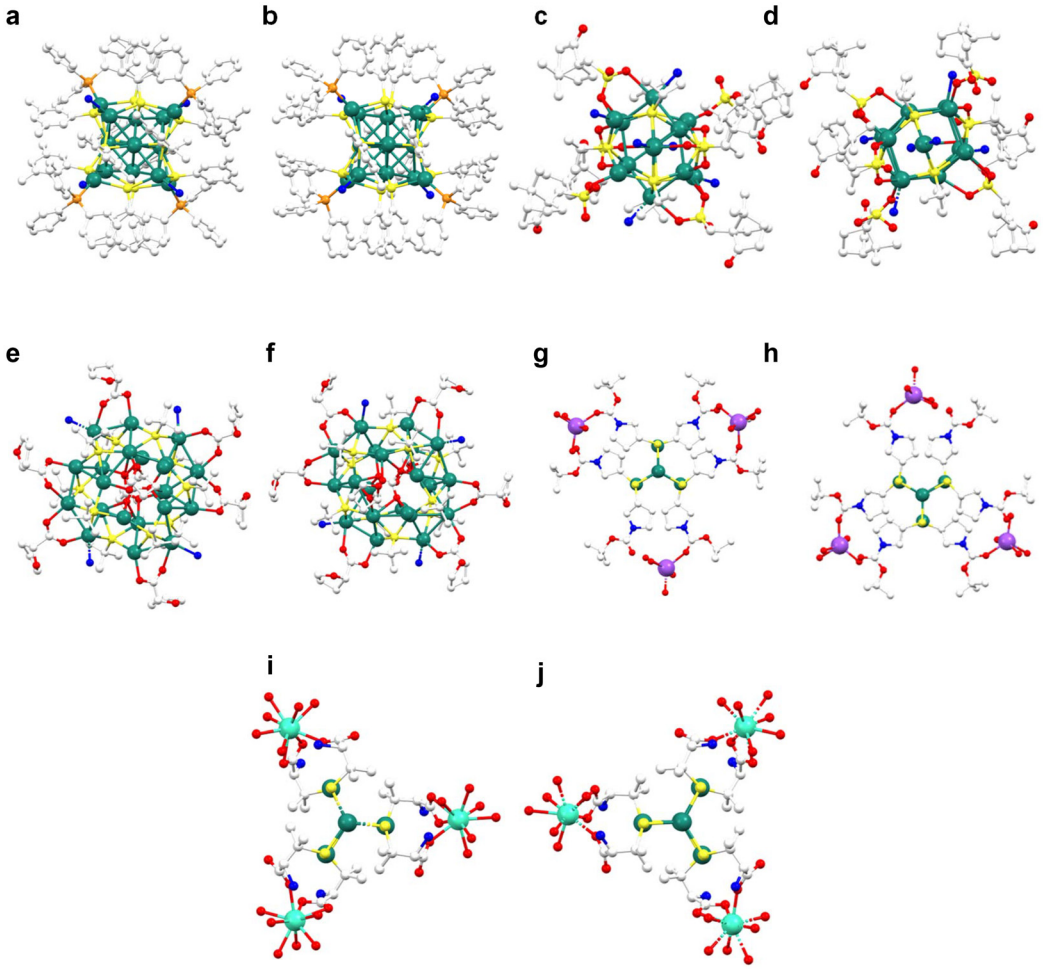

Fig. 4 Structural comparison of chiral units: (a) Ag_{14}LS; (b) Ag_{14}LR; (c) D-Ag_{12}An2Py; (d) L-Ag_{12}An2Py; (e) *R*-Ag_{20}bpy; (f) *S*-Ag_{20}bpy; (g) *R*-Ag_5-1; (h) *S*-Ag_5-1; (i) L-$LnAg_5$; and (j) D-$LnAg_5$ (green: Ag, yellow: S, white: C, blue: N, red: O, orange: P, purple: Na, and light green: Ln).

$3CF_3COO\}_n$ (hereinafter referred to as SD/Ag_{72}c) (pi-bipy: 1,4-bis(4-pyridinylmethyl)piperazine) obtained from the bipy/pi-bipy linker and $[PW_9O_{34}@Ag_{51}]$ clusters.[44] SD/Ag_{72}a exhibited a 2D structure, while SD/Ag_{72}c showed a 3D structure. Their respective space groups are $P2_1/n$ and $P\bar{1}$, respectively. Each node of SD/Ag_{72}a forms a bond with the other four nodes *via* a bipy linker, forming a network structure with a total of 11 bipy linkers (Fig. 2u). On the other hand, each node of SD/Ag_{72}c forms a structure *via* a pi-bipy linker with six different nodes, with four clusters bridged by one pi-bipy, one cluster bridged by two pi-bipy, and one cluster bridged by three pi-bipy linkers (Fig. 2v).

In 2023, Das, Negishi and colleagues reported the synthesis of a 2D SCAM, $[Ag_{12}(S^tBu)_6(CF_3COO)_6(bpva)_3]_n$ (bpva = 9,10-bis((2-pyridin-4-yl)vinyl)anthracene) (Fig. 3i) (hereinafter Ag_{12}bpva), and an 1D SCAM, $\{[Ag_{12}(S^tBu)_6(CF_3COO)_6(bpb)(DMAc)_2(H_2O)_2](DMAc)_2\}_n$ (bpb = 1,4-bis(4-pyridyl)benzene) (Fig. 3d) (hereinafter Ag_{12}bpb).[21] Each node is an Ag_{12} cluster and the core is $Ag_{12}S_6$, with S bridged to four different Ag atoms. The Ag_{12} nanoclusters in Ag_{12}bpva form a three-layered Ag_3S_3–Ag_6–Ag_3S_3 core, with the six Ag atoms in the middle layer acting as a six-linked node (Fig. 2h). The crystal system of this SCAM was monoclinic, and the space group was $P2_1/n$. On the other hand, the core of Ag_{12}bpb has a three-layer structure of Ag_5S_2–Ag_2S_2–Ag_5S_2 and is protected by two DMAc molecules and two water molecules, in addition to six CF_3COO^- ligands (Fig. 2f). The crystal system and space group of Ag_{12}bpb were the same as Ag_{12}bpva, monoclinic and $P2_1/n$. Both SCAMs were immersed in a variety of organic solvents followed by PXRD analyses, which corroborated the preservation of the crystalline structures after solvent treatment.

In the same year, Zang *et al.* reported a chiral SCAM, $\{[(Ag_{12}(^iSPr)_6$(D/L-CSA)$_6(An2Py)_3)]\cdot(H_2O)_2\}_n$ (CSA = camphor sulfonic acid) (hereinafter D-Ag_{12}An2Py, L-Ag_{12}An2Py),[45] by utilizing the bpva linker used by Das and Negishi *et al.* The node is composed of Ag_{12} nanoclusters, which form six coordination bonds and a net structure with 4 different nodes along the 2D space (Fig. 4c and d). The 2D SCAMs displayed the *AB* stacking pattern. The space group of the SCAMs was $P\bar{1}$ and the topology was characterized as **sql**.

A paper from Zang *et al.* reported the synthesis of $[(CO_3)@Ag_{20}(^tBuS)_{10}(R/S\text{-THF-COO})_8bpy_2]$ (hereinafter *R*/*S*-Ag_{20}bpy).[46]

The node of this SCAM is composed of Ag_{20} nanoclusters, with CO_3 derived from atmospheric CO_2 incorporated into the structure as an anion template. The cluster core is protected by ten ^{t}BuS$^-$ ligands, each forming a bond with four different Ag atoms. The core is also protected by eight *R*/*S*-THF-COO$^-$ ligands. Each node forms four coordination bonds (Fig. 4e and f). The authors also reported that a similar structure could be obtained by using bpy-NH_2 instead of bpy.

Thus, although only a short time has passed since the discovery of SCAMs, a variety of SCAMs with different structures have been reported. SCAMs using bidentate linkers revealed new structures upon changing the structure of the linker, structural transformation accomplished under specific conditions, and the construction of hybrid structures using SCAMs.

2.1.2 Tridentate linkers. The number of SCAMs utilizing tridentate linkers is small compared to the number of SCAMs using bidentate and tetradentate linkers. Here, we introduce the structures of tridentate linkers that have been reported at the present time.

In 2018, Wang, Zang and colleagues discovered $[Ag_{12}(S^tBu)_6(CF_3COO)_6(TPPA)_6\text{-}(DMAc)_x]_n$ (denoted as Ag_{12}TPPA·AA), a 2D SCAM, by using the tridentate linker tris(4-pyridylphenyl)amine (TPPA) (Fig. 2h and 3j).[47] This 2D SCAM is stacked in the *AA* fashion. However, there was a change in the PXRD peaks observed between the crystals in the mother solvent and after drying in air for some time. Intriguingly, this change was believed to be caused by the displacement of SBUs and the collapse of the *AA* stacking mode due to the desorption of DMAc from the structure upon drying in air. This was confirmed by SC-XRD measurements on the crystals after drying, which revealed that structural shrinkage occurred, resulting in a change in the *AB* stacking mode. More interestingly, after 6 hours of growth in the other solvent, this structure changed to an *ABC* stacking structure. Structural analysis of these crystals revealed that changes in the stacking mode caused changes in the crystal system and space group: the crystal system of Ag_{12}TPPA·AA was trigonal and the space group was $P\bar{3}$, for Ag_{12}TPPA·AB they were hexagonal and $P6_3/mmc$, and for Ag_{12}TPPA·ABC they were trigonal and $R\bar{3}m$. The distance between the layers became gradually shorter with each change to the *AA*, *AB*, or *ABC* stacking mode.

In 2023, Das and Negishi *et al.* reported $[Ag_{12}(S^tBu)_6(CF_3COO)_6(TPBTC)_6]_n$ (TUS 3) using the tridentate ligand, benzene-1,3,5-tricarboxylic acid tris-pyridin-4-ylamde (TPBTC) (Fig. 3k).[19] TUS-3 has linkers that form three coordination bonds, while the Ag_{12} nanoclusters form six bonds (Fig. 2h). The **kgd** topology was reported for the first time in SCAMs. SC-XRD analysis illustrated that the crystal system of TUS 3 was trigonal, and the space group was $R\bar{3}$. Uniaxial open channels arising from stacked 2D layers enabled an impressive Brunauer–Emmett–Teller (BET) surface area of 394 $m^2\ g^{-1}$. PXRD analysis showed that the structure of TUS 3 did not change when TUS 3 was exposed to dichloromethane, ethanol, 0.1 M NaOH, and 0.1 M HCl, suggestive of its structural stability.

In the same year, Wang, Zhang and colleagues reported $[Ag_{12}(S^tBu)_6(CF_3COO)_6(BDP\text{-}Py)_2]_n$, $[Ag_{12}(S^iPr)_6(CF_3COO)_6(BDP\text{-}H)_2]_n$, and $[Ag_{12}(S^iPr)_6(CF_3COO)_6(BDP\text{-}I)_2]_n$ (hereinafter Ag_{12}-BDP-Py, Ag_{12}-BDP-H, and Ag_{12}BDP-I).[48] The cluster node in each SCAM is composed of 12 Ag atoms, and each node forms coordination bonds with six different linkers. Each Ag_{12} nanocluster is stabilized by six S^tBu^- or S^iPr^- and six CF_3COO^- ligands. The net structures of Ag_{12}-BDP-Py (Fig. 3l), Ag_{12}BDP-H (Fig. 3m) and Ag_{12}BDP-I (Fig. 3n) are all forming 2D structures and all of their space groups are $P\bar{1}$. From the viewpoint of topologies, that of Ag_{12}-BDP-H and Ag_{12}BDP-I was **kgd** and the stacking mode was *AB* stacking. Besides, the thermal stability of Ag_{12}-BDP-H and Ag_{12}BDP-I until 163 °C and 175 °C were assessed by TGA measurements.

Thus, there are considerably fewer reported cases of SCAMs using a tridentate linker compared to the bidentate linker and the tetradentate linker. Therefore, SCAMs using tridentate linkers are novel and have great potential to become a hotspot of SCAMs in the future.

2.1.3 Tetradentate linkers. A number of SCAMs constructed by using tetradentate linkers have been reported so far. In 2019, Li, Zang and co-workers reported the synthesis of a new 3D SCAM, $[Ag_{12}(S^tBu)_6(CF_3COO)_6(CPPP)_2(DMAc)_{12}]_n$ Ag_{12}CPPP, CPPP = 2,5-bis(4-cyanophenyl)-1,4-bis(4-(pyridine-4-yl)-phenyl)-1,4-dihydropyrrolo[3,2-*b*]pyrrole (Fig. 3o).[49] The $Ag_{12}S_6$ core is unique in that it forms a three-layered Ag_4S–Ag_4S_4–Ag_4S structure, resulting in an interesting ligand binding scheme: there are six coordinating CF_3COO^- ligands, two of which form bonds to only one Ag atom, while the remaining four form bonds to three Ag atoms (Fig. 2k). There are eight sites where CPPP linkers can form coordination bonds with the cluster node, and four sites are coordinated by the nitrile group and the remaining four sites are coordinated by the pyridine group. These unique results indicate that Ag_{12}CPPP has a new geometrical structure, $(4^{28})(4^6)_2$. Looking at the crystal system and space group, the linker CPPP is monoclinic and the space group is $P2_1/n$, while A_{12}CPPP has the same crystal system but the space group is $I2/m$. TGA revealed the presence of 12 DMAc molecules in the structure of the SCAM; however, the molecules could not be successfully identified within the structure. As evidenced by the PXRD results, the crystalline structure of Ag_{12}CPPP was maintained even after the SCAM was left for 60 days at room temperature or after removal of DMAc molecules.

In 2019, Wang, Zang and colleagues successfully synthesized $[Ag_{12}(S^tBu)_6(CF_3COO)_3(TPyP)]_n$ (Ag_{12}TPyP, TPyP = 5,10,15,20-tetra(4-pyridyl)porphyrin, Fig. 3p).[22] The $Ag_{12}S_6$ cluster core of Ag_{12}TPyP showed a structure forming only four coordination bonds (Fig. 2j), unlike the usual core forming six coordination bonds. Ag_{12}TPyP formed a 2D structure by coordination bonding of the linker to four different cluster nodes and showed an *AB* stacking pattern. The crystal system of Ag_{12}TPyP was triclinic and the space group was $P\bar{1}$. The crystal structure of Ag_{12}TPyP after immersion in many organic solvents for 36 hours or left in the air for 3 months did not collapse, indicative of the high stability of the structure.

In the same year, the synthesis of $\{[Ag_{12}(S^tBu)_6(CF_3CO_2)_6(tppe)_{1.5}](DMAc)_{39}\}_n$ (tppe = 1,1,2,2-tetra-

kis(4-(pyridine-4-yl)phenyl)ethane, Fig. 3q) (hereinafter named Ag_{12}tppe ⊃ DMAc) was reported by Li, Zang and colleagues.[24] This structure consists of a node with an $Ag_{12}S_6$ core and a tetradentate linker TPPE, but what is remarkable is the large pore size (32 Å). ^{1}H NMR spectra obtained after the incorporation of D-menthol, L-menthol, 4,4-dimethoxybenzil, and 3,6-di(2-thienyl)diketopyrrolopyrrole as guest molecules showed that the guest molecules were encapsulated in the SCAM structure; however, PXRD observations indicated no structural change with the introduction of any of the guest molecules. The structural analysis by SC-XRD showed that the crystal system of Ag_{12}tppe ⊃ DMAc was cubic and the space group was $Pm\bar{3}m$.

In the same year, Zang, Tang and colleagues reported the successful synthesis of an innovative SCAM. The SCAM stands out owing to the existence of two kinds of Ag nanocluster nodes.[50] The chemical formula of this SCAM is $\{[Ag_{12}(S^tBu)_6(CF_3CO_2)_6]_{0.5}[Ag_8(S^tBu)_4(CF_3CO_2)_4](tppe)_2(DMAc)_{10}\}_n$ (hereinafter $Ag_{12}Ag_8$tppe). The number of DMAc molecules in the SCAM structure was determined by TGA, elemental analysis, and ^{1}H NMR spectroscopy. Ag_8 nanocluster nodes are forming six coordination bonds (Fig. 2a). On the other hand, the Ag_{12} cluster is a three-layered node of Ag_3S_3–Ag_6–Ag_3S_3, with six S^tBu^- and six CF_3COO^- as ligands, forming four coordination bonds with tppe, as evidenced by structural analysis (Fig. 2l). The tppe bridging clusters formed a 3D structure by coordinating with three Ag_8 clusters and one Ag_{12} cluster per linker molecule; the type of geometric structure of $Ag_{12}Ag_8$tppe was $\{4^2\cdot8^4\}\{4^3\cdot6^2\cdot8\}_4\{4^9\cdot6^6\}_2$. Different from Ag_{12}tppe, $Ag_{12}Ag_8$tppe displayed the crystal system and space group as triclinic and $P\bar{1}$, respectively.

In 2020, Cui, Sun and co-workers successfully synthesized $\{[Ag_{27}S_2(^tBuS)_{14}(CF_3COO)_8(TPyP\text{-}H_2)][(CF_3COO)\}_n$ (Ag_{27}-MOF) using a TPyP linker,[25] which Zang *et al.* used to synthesize another SCAM.[22] This SCAM has an Ag_{27} cluster core protected by 14 S^tBu^- and 8 CF_3COO^- ligands (Fig. 2t). To reduce the steric hindrance of TPyP, only four of the 27 silver atoms form coordination bonds with the linker, and the structure is expanded along 2D space. PXRD measurements were also performed to determine whether the crystal structure is affected by aging (4 months) and solvent immersion, and it was confirmed that none of the peaks changed. Structural analysis showed that the crystal system of the Ag_{27}-MOF was orthorhombic, and the space group was *Cmcm*.

In 2022, Wang, Zang and colleagues reported $[Ag_9(^tBuC{\equiv}C)_6(CF_3COO)_3(AgTPyP)]_n$, (hereinafter Ag_9-AgTPyP).[26] This structure was found to be 2D composed of Ag_9 clusters (Fig. 2b) as a node forming four coordination bonds and having an *AB* stacking structure (Fig. 5c). Structural analysis revealed that this node has six ^{t}BuC≡C ligands in two types of bonding modes, σ-type and π-type, and three CF_3COO^- ligands are coordinated to two Ag atoms. On the other hand, focusing on the tetradentate linker TPyP, a very interesting structural change occurred. The Ag atom forms a complex with TPyP at the synthesis stage. The crystal system of this SCAM was monoclinic, and the space group was *C*2/*c*. PXRD measurements of Ag_9-AgTPyP after immersion in water for 24 hours and in air for 5 months showed no detectable change in its peaks.

In 2023, Das and Negishi *et al.* used the linkers 1,1,2,2-tetrakis(4-(pyridin-4-ylethynyl)phenyl)ethane (TPEPE, Fig. 3r) and 1,1,2,2-tetrakis(4-((*E*)-2-(pyridin-4-yl)vinyl)phenyl)ethane (TPVPE, Fig. 3s) to prepare $[Ag_{12}(S^tBu)_6(CF_3COO)_6(TPEPE)_6]_n$ (TUS 1) and $[Ag_{12}(S^tBu)_6(CF_3COO)_6(TPVPE)_6]_n$ (TUS 2).[33] Both SCAMs revealed 3D structures, and both form Ag_{12} nodes of the same shape, allowing for the formation of six coordination bonds with the linkers (Fig. 2h). SCXRD structural analysis showed that the crystal system of both TUS 1 and TUS 2 was trigonal and the space group was $R\bar{3}c$. To confirm the structural stability against solvents, TUS 1 and TUS 2 were placed in toluene, dioxane, chloroform, acetone, and water followed by PXRD studies which displayed no obvious change in the peaks.

In 2024, the same research group presented the synthesis of 3D $[Ag_{12}(S^tBu)_6(CF_3COO)_6(TPSBF)_6]_n$ (designated as TUS 4) (TPSBF = 2,2′,7,7′-tetra(pyridine-4-yl)-9,9′-spirobi(fluorene)) (Fig. 3t).[32] The Ag_{12} cluster core has a three-layer structure of Ag_3S_3–Ag_6–Ag_3S_3, with the six Ag atoms in the middle layer, cubic and the space group was $Pn\bar{3}n$. The SCAM structure was found to collapse after grinding. This was determined by changes in PXRD before and after grinding. Solid-state UV-vis absorption spectra, solid-state emission spectra and Raman spectra of the ground SCAM sample were comparable to the respective spectra of the linker. In addition, it was necessary to add $NaBH_4$ to TUS-4 in order to use it for surface-enhanced Raman scattering (SERS) application, but the PXRD peaks did not change significantly before and after the addition of $NaBH_4$, indicating that the crystal structure was not changed by the addition of the $NaBH_4$ reducing agent.

As described above, it was confirmed that SCAMs using tetradentate linkers are no less than SCAMs using bidentate linkers. The structure of SCAMs with tetradentate linkers can be 2D or 3D, making them more complex than with bidentate linkers.

2.1.4 Multidentate linkers (points of extension more than 4). Here we show SCAMs with linkers having points of extension more than four. In 2023, Das and Negishi *et al.* adopted the linker *N*,*N*,*N*′,*N*′,*N*″,*N*″-hexa(pyridine-4-yl)benzene-1,3,5-triamine (hpbt) (Fig. 3u) to prepare a 3D SCAM $\{[Ag_{10}(S^tBu)_6(CF_3COO)_4(hpbt)](DMAc)_2(CH_3CN)_2\}_n$ (Ag_{10}hpbt).[21] The core of this cluster node is $Ag_{10}S_6$, of which the major part is Ag_8S_6, and the other two Ag atoms are held together by weak bonds with S atoms (Fig. 2d). The Ag_{10}hpbt used a 6-connected linker, and at present, there are no known SCAMs built with linkers with a higher coordination number than this. SC-XRD results indicated that the crystal system of this SCAM was monoclinic and the space group was *C*2/*c* (Fig. 5d).

Currently, only bidentate, tridentate, tetradentate, and hexadentate linkers have been reported in SCAMs, and there is only one reported case of a SCAM constructed from a hexadentate linker. Therefore, the SCAM formed by using a hexadentate linker features high novelty. In addition, from the viewpoint of linker symmetry, there is a good possibility that SCAMs can be synthesized using linkers with even higher denticities.

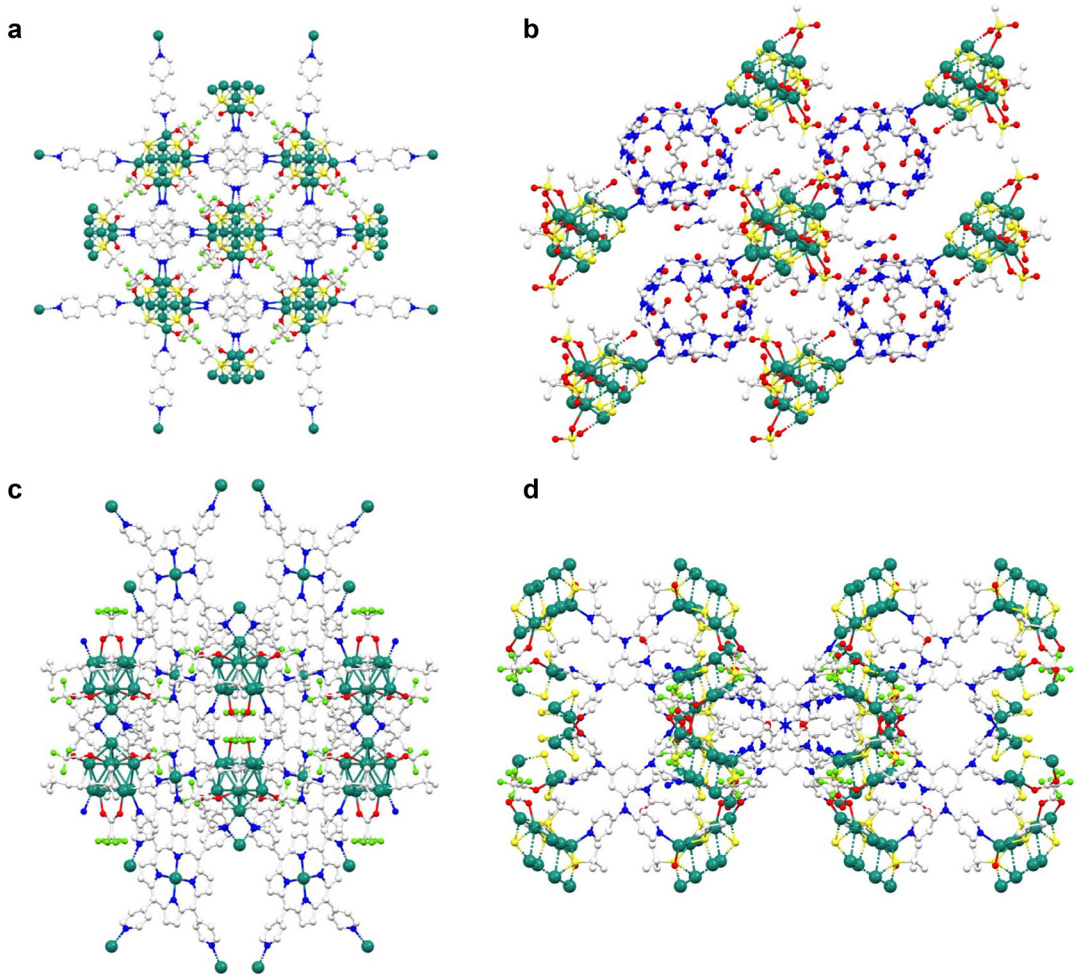

Fig. 5 Extended structure of SCAMs; (a) Ag_{12}bpy (2D), (b) SCM 3 (1D), (c) Ag_9-AgTPyP (2D), and (d) Ag_{10}hpbt (3D) (white: C, blue: N, red: O, light green: F, green: Ag, and yellow: S).

2.2 SCAMs formed by Ag–O bonds

The number of reported examples of SCAMs with Ag–O bonds is small compared to SCAMs constructed with Ag–N bonds. Despite that some SCAMs synthesized by using pyridyl linkers show good stability, a lack of generalizability exists.[20] On this account, using carboxyl groups can augment the stability of the SCAMs than when using a pyridyl linker.[20] Here we describe the reported SCAM structures constructed from Ag–O bonds.

2.2.1 Bidentate linkers. Several SCAMs using bidentate carboxyl linkers have been reported to date because of their relatively simple structures. In 2020, Dong, Zang and co-workers successfully synthesized $\{[Ag_6(S^tBu)_4(L)]\cdot guest\}_n$ (denoted as AgS-L) by using the 2,3,5,6-tetrafluorobenzene-1,4-dicarboxylate (H_2L) linker.[51] SC-XRD analysis revealed that the SCAM adopts a 3D structure due to the presence of a chain of SBUs, which are bridged by linkers. AgS-L possesses an orthorhombic crystal system, with the space group $I2_12_12_1$. The S atoms have two coordination patterns, one is tetra-coordinated, in which the Ag forming the coordination bonds develop a distorted square configuration. The other coordination bond pattern is three-coordinated, and the Ag atoms that form coordination bonds have a triangular configuration. The chain-like structure was extended along the *a*-axis, and the size of the channel generated in the *bc* plane was 9.2 × 9.5 Å^2. The 3D chiral SCAM structure has a point symbol $\{10^3\}$. The distribution of fluorine atoms and alkyl groups of S^tBu in the inner surface of the pore channels indicated hydrophobicity.

In 2021, Morsali *et al.* reported the successful synthesis of $\{Ag_{14}[O_2C\text{-}(CF_2)_4CO_2]_4(SPr^i)_6(DMF)_6\}_n$ (SSc-2).[52] This structure was found to consist of Ag_{14} cluster nodes bridged *via* octafluoroadipic acid linkers. SC-XRD analysis revealed that the cluster core was composed of 14 Ag atoms and six S atoms of the SPr^{i-} ligands. The SCAM adopted the orthorhombic crystal system and the space group *Pccn*.

In another study, the same research group reported the synthesis of SCAM with the formula $[Ag_{14}(SPr^i)_6(C_9F_{14}O_4)_4(DMF)_8]_n$ (SPc).[53] Like SSc-2, its core is composed of 14 Ag atoms and six S atoms of the SPr^{i-} ligands, which are protected by eight DMF molecules. The 2D SCAM sheets extend in the *ac*-plane, with no interpenetration between the sheets and the distance between

the 2D sheets as 1.02 nm. The crystal system of SPc was triclinic, and the space group was $P\bar{1}$.

In 2023, $[Ag_{12}(S^iPr)_6(D/L\text{-}CSA)_6(MeOH)_4]_n$ was reported by Duan, Zang and colleagues.[45] This SCAM structure is spread over one dimension. Each S^iPr^- ligand is bonded to four different Ag atoms, and each CSA^- forms bonds with two or three silver atoms. Structural analysis revealed that each cluster node is bridged by two CSA^- and the number of CSA^- that connected with each node is four.

As shown above, the number of SCAMs using bidentate carboxyl linkers is far fewer than those using pyridine linkers. Besides, the reports are relatively recent. Therefore, SCAMs synthesized by using bidentate carboxyl linkers are of great novelty, and further development is expected in the future.

2.2.2 Tetradentate linkers. Similar to bidentate linkers, several SCAMs using tetradentate linkers with carboxyl groups have been reported. In 2022, Zang *et al.* reported the synthesis of $[Ag_6(^iPrS)_4(BTEC)_{0.5}]_n$ (hereinafter referred to as Ag_6BTEC), a chain of SBUs bridged by tetradentate carboxylic acid, 1,2,4,5-benzenetetracarboxylic acid (H_4BTEC) linkers.[54] Two methods were reported for the synthesis of Ag_6BTEC: (i) a method in which the chain complex $[Ag_4(^iPrS)_3(CF_3COO)]_n$ and the linker were dissolved in acetonitrile/ethanol followed by heating, and (ii) a one-pot synthesis method in which the precursors $AgNO_3$, $[^iPrSAg]_n$, and the linker were added in acetonitrile/ethanol and heated. The resulting crystal, Ag_6BTEC, shows a wavy structure of $(–Ag–S–)_n$ layers, a chain-like polymer composed of Ag and S atoms, with the S atoms forming bonds with three or four Ag atoms. Ag_6BTEC exhibited a monoclinic crystal system and the space group was $P2_1/n$. The carboxyl groups of H_4BTEC are all deprotonated. Ag_6BTEC was found to be thermally stable up to 240 °C based on variable-temperature PXRD and TGA characterization.

In the same year, Wang, Zang and co-workers reported the synthesis of $[(HPO_4)_4(H_2PO_4)_2@Ag_{54}(^iPrS)_{32}(CF_3COO)_6(CH_3CN)_2(H_2TCPP)(TCPP)]_n$, (hereinafter ZZU-601; H_2TCPP = tetrakis(4-carboxyphenyl)porphyrin) and $\{[(HPO_4)_2@Ag_{18}(^iPrS)_8(H_2PO_4)_4(H_2ZnTCPP(C_2H_5OH))]\cdot 2CH_3CN\}_n$, (hereinafter ZZU-602; ZnTCPP = 5,10,15,20-tetrakis(4-carboxyphenyl)porphyrinato-Zn(II)).[55] ZZU-601 had four $[HPO_4]^{2-}$ ions and two $[H_2PO_4]^-$ ions acting as anion templates for 36 silver atoms, and the Ag_{54} cluster node was protected by 32 $^iPrS^-$. Although there was a total of eight TCPP linkers bridging the Ag_{54} nanoclusters, the coordination of four TCPP linkers in two planes resulted in a 2D planar extension, finally forming a 3D structure for ZZU-601 as a whole. On the other hand, in ZZU-602, two $[HPO_4]^{2-}$ acted as anion templates and the core was protected by 10 $^iPrS^-$ ions and four $[H_2PO_4]^-$ ions. Overall, this SCAM structure exhibited 2D extension after being connected by ZnTCPP linkers. The crystal system of both ZZU-601 and ZZU-602 was triclinic, and the space group was $P\bar{1}$.

Thus, there are only a few reported examples of the synthesis of SCAMs utilizing carboxylic acids as tetradentate linkers in the last one or two years. Therefore, it can be said that SCAMs using tetradentate linkers that make Ag–O bonds have a short history and are still a developing field.

2.3 SCAMs formed by Ag–S bonds

Attempts have been made to synthesize SCAMs by using S as an electron-donating group like N, but the HSAB rule theoretically makes it impossible to synthesize SCAMs with Ag–S bonds due to the problem that precipitation occurs too rapidly.[20]

However, in 2018, Duan *et al.* created a stir against this *status quo*. They were the first to report an Ag–S-bonded SCAM by using the tridentate thiourea linker 2,2′,2″-((((1,3,5-triazine-2,4,6-triyl)tris(azanediyl))tris(benzene-4,1-diyl))tris(ethan-1-yl-1-ylidene))tris(hydrazinecarbothioamide) to form TNS-Ag_8 SCAM and 2,2′,2″-((((1,3,5-triazine-2,4,6-triyl)tris(oxy))tris(benzene-4,1-diyl))tris(methanylidene))tris(hydrazine carbothioamide) to form the TOS-Ag_4 SCAM.[56] The Ag atoms in TNS-Ag_8 are bonded to three different S atoms and are located at the center of a plane consisting of three S atoms. The clusters are also bridged by forming Ag–S bonds, but the S atoms are bridged to two Ag atoms. The core of the TNS-Ag_8 cluster is Ag_8S_{12}, which means that 12 ligands are coordinated to the eight Ag atoms. Two linkers are used to connect three different clusters. In other words, the clusters are nodes that form coordination bonds with six pairs of linkers. This SCAM has a 3D structure, and the clusters can be regarded as a six-linked node. Besides, there are two types of pores due to this particular structure. Structural analysis revealed that the crystal system of TNS-Ag_8 is cubic, and the space group is $Pa\bar{3}$. On the other hand, in TOS-Ag_4, tetrahedral clusters form coordination bonds as 3-linked nodes, forming a doubly interpenetrated 3D structure. The core of this cluster is Ag_4S_6, and the Ag atoms form coordination bonds with the six S atoms. Each S atom is located on an edge of the tetrahedron and is bridged to two Ag atoms. The number of linkers bridging the clusters is six per cluster. This means that two linkers form a structure bridging three clusters, which is also the same as in TNS-Ag_8. The resulting SCAM structure is 3D, and the silver nanoclusters can be said to behave as a three-linked node. As a result, TNS-Ag_4 also has two types of pores. Structural analysis showed that the crystal system of TOS-Ag_4 is cubic, as in TNS-Ag_8, and the space group is $P2_13$.

In 2022, Si, Zang and co-workers succeeded in synthesizing a SCAM with Ag–S bonds by developing a new approach. The reported SCAM has the structure $[NaAg_5(R/S\text{-}L)_6(H_2O)_2(CH_3OH)]Na[Ag_5(R/S\text{-}L)_6]$ (R-Ag_5-1, S-Ag_5-1) (R-L,S-L = R/S-*tert*-butyl-3-mercaptopyrrolidine-1-carboxylate), which is a 2D structure of Ag_5 nanoclusters cross-linked by forming coordination bonds with Na ions (Fig. 4g and h).[57] The 2D structures were stacked in the *AA* fashion to form channels along the *c*-axis. Looking at the nanoclusters composing the node, its core structure was Ag_5S_6, with a triangular prism formed by six S atoms. Each S atom formed a coordination bond with two different Ag atoms, and the five Ag atoms were located at the center of the top and bottom faces or at the center of the sides of the triangular prism composed of six S atoms, thus forming a twisted triangular biconical structure. On the other hand, the Na ions forming the bridging structure

formed coordination bonds with the two carboxyl groups of the ligands of the two Ag_5 nanoclusters, two molecules of water, and one molecule of methanol, for a total of five molecules. There are six ligands with carboxyl groups around the cluster that can coordinate with sodium, and three of them form coordination bonds with sodium: two from the ligands on the same base of the triangular prism and one from the ligand on the other base. The remaining three carboxyl groups that are not used for coordination bonds with sodium may form hydrogen bonds with water molecules. Interestingly, in addition to the Ag_5 nanoclusters that make up a SCAM, there are also Ag_5 nanoclusters in the channels, which are stabilized by forming hydrogen bonds with the backbone of the structure. The crystal system of both was trigonal and the space group was *P*3. The PXRD peaks of this SCAM showed that the structure changed to $Na[Ag_5(R/S\text{-}L)_6]$ by desorption of the water molecules and methanol molecules that form the backbone upon drying.

In 2023, taking a similar approach to Zang *et al.*, Cao, Zheng and colleagues synthesized a new SCAM with an Ag–S bond. They used lanthanides, instead of sodium, to obtain $\{[LnAg_5(\text{L-HL})_6]\cdot(ClO_4)_2\cdot xH_2O\}_n$ (L-/D-HL = L-/D-penicillamine) (L-$LnAg_5$-1: Ln = Gd, x = 15, L-$LnAg_5$-2: Ln = Eu, x = 15, L-$LnAg_5$-3: Ln = Tb, x = 11) and $\{[LnAg_5(\text{D-HL})_6]\cdot(ClO_4)_2\cdot yH_2O\}_n$ (D-$LnAg_5$-1: Ln = Gd, y = 12, D-$LnAg_5$-2: Ln = Eu, y = 24, D-$LnAg_5$-3: Ln = Tb, y = 12) (Fig. 4i and j).[58] The SCAMs have a chiral Ag_5 cluster with C_3 symmetry bridged by three different lanthanides as inorganic ligands. The core structure of the cluster is Ag_5S_6, in which the five Ag atoms are arranged to form a shape like two triangular pyramids combined, and the six linkers with S bind two different Ag atoms. The Gd in L-$LnAg_5$-1 is coordinated by nine O atoms, which are derived from the carboxyl groups possessed by the six L-HL^- ligands. Next, L-$LnAg_5$-1 was immersed in a wide variety of organic solvents, and PXRD showed that no structural changes occurred. The crystal system and space group of all L-$LnAg_5$-1, L-$LnAg_5$-2, L-$LnAg_5$-3, D-$LnAg_5$-1, D-$LnAg_5$-2, and D-$LnAg_5$-3 are cubic and $P2_13$.

As described above, SCAMs with Ag–S bonds can be divided into two main types: one is bridged by thiourea linkers, which was the first SCAM to be bridged by Ag–S bonds. The other is a thiol-protected ligand that acts as an inorganic linker by using a different metal to expand the structure of the ligand. Both SCAMs have very interesting structures, and the latter is expected to be diverse depending on the type of thiol ligand used and the metal species used to act as the inorganic linker.

2.4 SCAMs formed by special types of coordination bonds

The SCAMs shown so far were discussed separately in terms of the type of bonding. Here we discuss SCAMs that have additional intricacy by combining two different types of bonding.

In 2019, Liu, Chen and colleagues reported $[Ag_7(tza)_3(Htza)_2(H_2tza)(H_2O)]$ (hereafter $Ag_7tza(H_2O)$), a new SCAM with unprecedented complexity by using 1*H*-tetrazole-5-acetic acid (H_2tza).[59] Silver atoms belonging to the Ag_7 cluster, which corresponds to the node of this SCAM, have three different states: the first is silver atoms coordinating with N atoms having four different linkers. There are two atoms of this type. The second is a silver atom coordinating with the N atoms of three different linkers and there are two silver atoms that have this arrangement; the third is a silver atom in coordination bonds with both N and O atoms and the remaining three are silver atoms that fall into this category. This silver atom forms coordination bonds with three N atoms and one O atom, and the silver atom is located in the distorted triangular pyramid. In contrast, the next step is to look at the bonding mode of H_2tza. It was found that the coordination structure of the linker, H_2tza, also has three different states. There are three types of coordination structures: a structure in which four N atoms in the tetrazole ring bond to four different silver atoms, a structure in which three out of four N atoms of the tetrazole ring bond to three different silver atoms, and a structure that connected with five different Ag atoms bonding with a carboxyl group in addition to the tetrazole ring. The coordination structures of the silver atoms and linkers in these various states create a unique 3D structure. This crystal system was triclinic, and the space group was $P\bar{1}$.

3 Applications of SCAMs

3.1 In sensing

In 2017, Zang and co-workers reported a Ag_{12}bpy SCAM with unique turn-off fluorescence switching in response to oxygen and turn-on vapochromic switching in response to volatile organic compounds.[18] On the basis of the Stern–Volmer plot, the SCAM exhibited a limit of detection (LOD) of 32 Pa for oxygen at 1% quenching. Moreover, Ag_{12}bpy treated with ethanol vapor showed a significant increase in photoluminescence intensity by 26 times compared to air (off state). In 2018, the same research group presented Ag_{10}bpy as a solvatochromic sensor for the detection of chloromethanes.[60] Each chloromethane showed a different fluorescence response, thereby enabling the SCAM to distinguish the chemicals. This turn-on luminescence switching was caused by the gate-opening effect. Hence, Ag_{10}bpy with solvents manifested different chromic variations within 83–293 K. In 2019, they reported Ag_{18}bpy-NH_2 which showed different photoluminescence behavior after grinding, and the blue emission of the pristine sample was recovered again after fuming with EtOH and acetone.[61] Pristine Ag_{18}bpy-NH_2 demonstrated an emission spectrum centered at 458 nm, and the emission peak was shifted to 491 nm post-grinding. This phenomenon was assumed to stem from inter-chain bpy-NH_2 interaction. As substantiated by PXRD analysis, the crystallinity of the SCAM could be recovered again after treatment with EtOH/acetone. In another study, reversibly photoswitchable Ag_{10}bpy was utilized for the sensing of acetonitrile (CH_3CN).[34] Ag_{10}bpy soaked with CH_3CN showed green emission; however, the intensity of the emission declined gradually up to quenching after removing the CH_3CN which could be recovered instantaneously

upon treating the sample with CH_3CN. The cycling tests for its switchable turn-on/off luminescence divulged that the SCAM could undergo reversible structural change for at least 20 cycles. In 2020, the Ag_{12}bpy-NH_2 SCAM was adopted for oxygen sensing.[62] Owing to the dual-emitting (fluorescence and phosphorescence) behavior of Ag_{12}bpy-NH_2, the ratio of fluorescence to phosphorescence (that depends on oxygen concentrations) was checked at different oxygen levels. As a result, a detection limit of 11.4 mPa was attained (this LOD was only 3.56×10^{-6}% of Ag_{12}bpy). In 2022, Pradeep *et al.* utilized the AgNC-MOF for the fluorescence sensing of nitroaromatics.[63] The AgNC-MOF was soaked in some solvents, and the photoluminescence results showed that the intensity dramatically decreased when it was exposed to 2,4-dinitrotoluene and 2-nitrotoluene. Furthermore, after it was placed in an oven for 20 min at 45 °C, its emission was recovered. In 2023, Das, Negishi and colleagues introduced two SCAMs designated as TUS 1 and TUS 2 for the detection of Fe^{3+} in water.[33] The LOD of Fe^{3+} was evaluated to be 0.05 nM L^{-1} for TUS 1 and 0.86 nM L^{-1} for TUS 2. These SCAMs were used to identify other metal ions as well, albeit finally futile. Accordingly, these SCAMs revealed superb selectivity towards Fe^{3+}. In 2024, the same laboratory reported TUS 4 for detecting Hg^{2+}.[32] This detection of Hg^{2+} ions was verified by SERS, and TUS-4 showed the LOD of 0.07 pg mL^{-1}. The Raman spectral intensity with different ions was also inspected using the same protocol, and the results suggested that only after adding Hg^{2+}, the intensity was changed.

3.2 In catalysis

During World War I, mustard gas was used as a life-threatening warfare agent by the German military and brought over 4000 military deaths; hence, detoxification of this toxic gas is important for our health.[64] In 2019, Zang and colleagues reported the Ag_{12}TPyP SCAM as a photocatalyst for detoxifying 2-chloroethyl ethyl sulfide (CEES).[22] Under LED light irradiation and an O_2 atmosphere ($t_{1/2}$ = 1.5 min), this SCAM showed exemplary performance in converting 98% of CEES (1% loading) to CEESO within only 4 min. Besides, the catalytic activities of the Ag_{12} nanocluster, Ag_{12}bpy-2, TPyP and Ag-TPyP were also assessed for comparative analysis. As a result, Ag_{12}TPyP capably showed superlative performance and the conversion rate reached 100% at only 5 min, which revealed that the interaction between the Ag_{12} cluster and TPyP molecules is crucial to $^1O_2$ generation.

As a greenhouse gas, CO_2 has a pronounced impact on global warming; so many research efforts have been devoted to using CO_2 as the starting material for organic reactions.[65] Sun *et al.* adopted the Ag_{27}-MOF as a catalyst for CO_2-cycloaddition organic reactions.[25] The exposed silver nodes promoted the Ag···π interactions which in turn helped in activation of the C=C bonds. The result of CO_2-cycloaddition of the benzyl-prop-2-ynylamine reaction showed that the Ag_{27}-MOF indicated higher activities than other Ag compounds and precursors. Additionally, the Ag_{27}-MOF could be reused as a catalyst at least four times with the yield maintained over 90%. Various propargylamine (PA) substrates were used as the starting materials of the reaction and the following correlations were found: terminal PA substrates that have *N*-alkyl groups could get products in high yields, internal PA substrates also reacted and the products were the *Z* isomers.

A recent paper from Das, Negishi and co-workers reported the TUS 3 SCAM as a catalyst for reduction of $Fe(CN)_6^{3-}$ utilizing $NaBH_4$ in an aqueous medium.[19] Deriving from the structural order of the framework, aggregation problems usually occurring with silver nanoparticles as catalysts could be avoided and the stability enhanced. The reaction was monitored by UV-Vis absorption spectroscopy which was able to record the diminution of the $Fe(CN)_6^{3-}$ peak. When the concentration of this SCAM was increased from 0.1 to 1 nM, the reaction rate was obviously increased. Furthermore, the recyclability of the catalyst was validated by Fourier-transform infrared spectroscopy and powder X-ray diffraction which confirmed that TUS 3 could be used at least 4 times.

3.3 In biomedicine

Bacterial resistance ensuing from the misuse and overuse of antibiotics has put public health in serious peril and accounted for 1.27 million deaths globally in 2019.[66,67] A fascinating work from Zang and co-workers reported the synthesis of Ag_9-AgTPyP SCAM comprised of silver porphyrin units that harvest visible light for electron transfer to the Ag_9 clusters so as to allow O_2 activation to generate reactive oxygen species (ROS).[26] A surge in ROS concentrations could result in oxidative stress damage to lipids, proteins, nucleic acids and other cellular components, leading to bacterial cell death. Consequently, Ag_9-AgTPyP demonstrated notable antibacterial efficacy with 99.99999% against *S. aureus* after 90 min and 99.999% against *E. coli* after 120 min of visible light exposure. Taking a step further, this paper considered the competency of the SCAM film in personal protective equipment that also exhibited prominent antibacterial activity against multidrug resistant superbugs.

Integrating the high sensitivity and contrast of optical imaging with the high penetration depth and spatial resolution of ultrasound imaging,[68,69] photoacoustic imaging is a non-invasive diagnostic imaging technique which produces ultrasonic waves upon irradiation of the tissue by pulsed laser irradiation and reconstructs the absorption distribution of the tissue.[68,70] The applicability of a Ag_{14} cluster based SCAM in photoacoustic imaging was studied by Mandal and colleagues.[39] Strategically, a continuous-wave laser beam was utilized together with a pulsed laser beam to irradiate the sample in order to elevate the temperature of the sample selectively in a predetermined region of interest,[71] which thereby led to photoacoustic signal amplification over 85%.[39] A transparent glass tube loaded with the SCAM dissolved in ethanol/acetonitrile was inserted through a chicken breast tissue at a depth of *ca.* 2 mm to visualize the blood-vessel mimicking ability of the SCAM inside the tissue.[39]

The detection of nucleic acids is critical to ensuring point-of-care diagnostics and in genomics research. The majority of

the detection approaches are label-based that furnish very good sensitivity. On the other hand, the label-free detection approaches have made the analytical method easier by excluding labeling steps, thereby showing superiority in speed, convenience and cost-efficiency.[72] Negishi and co-workers achieved label-free detection of HIV-1 DNA by allowing a single-stranded DNA (ssDNA) probe to hybridize to target DNA sequences and two novel SCAMs in the role of a quencher to reduce the large background signal of ssDNA probes with SYBR Green I.[73]

4 Future vision

In the final section, we outline some potential research directions that can enable the future progress of this research field:

4.1 Understanding SCAM crystallization at the molecular level

Even though several SCAMs have been studied by many researchers, the crystallization mechanism underpinning SCAM synthesis still remains abstruse owing to the inadequacy of systematic assessment of the SCAM crystal nucleation and growth process. To overcome this lacuna, we can track the crystallization pathway by *in situ*/*operando* characterization approaches such as *in situ* XRD, *in situ* NMR spectroscopy, *in situ* transmission electron microscopy (TEM), *in situ* time-resolved high-resolution mass spectrometry, *etc*. The newly emerged CLASSIC NMR (Combined Liquid- And Solid-State *In situ* Crystallization NMR) technique enables one to get information on the evolution of solid and liquid phases concomitantly as a function of time throughout crystallization.[74,75] Furthermore, the lack of comprehension and control of SCAM crystallization poses a challenge to growing single crystals of adequate size to get good diffraction data by SCXRD. The advent of the cryo-electron microscopy-based technique *viz*. microcrystal electron diffraction (MicroED) enabled fetching of the structural information even if the crystal sizes are one-billionth the size required for X-ray diffraction.[76]

4.2 Photoluminescence of SCAMs

From a knowledge of the average lifetime and quantum yield of SCAMs determined using time-correlated single-photon counting (TCSPC), it is possible to categorize their luminescence as either phosphorescence or fluorescence. If the luminescence behavior of the SCAMs is characterized as phosphorescence, this is associated with a spin multiplicity of 3 which can be utilized for singlet oxygen generation and photon upconversion. The flexibility of the organic linkers plays a major role in internal conversion (IC) which affects the nonradiative rate constant, which in turn largely dictates if a SCAM can exhibit photoluminescence or not.

4.3 Introduction of silver clusters into covalent organic frameworks (COFs) to develop silver cluster–covalent organic frameworks (SCCOFs)

The coordination bond does not impart the SCAMs with adequate durability to withstand harsh operating conditions. To bring the open metal sites of SCAMs performing as absorption or active sites and the robustness of covalent bonds together under one roof, it might be rewarding to integrate silver clusters into COFs to construct SCCOFs. Given that the conventional synthesis of COFs relies on the solvothermal method which involves a high temperature (85–250 °C) while SCAMs are commonly prepared by slow evaporation of the reaction mixture at room temperature or low temperature (5–10 °C), a one-pot synthesis route might not be desirable for the preparation of SCCOFs owing to the thermal stability and solubility issues of silver precursors. As another option, post-synthetic metalation on a pre-synthesized COF network comprising linkers and bonds that contain electronegative elements (N, S, O) serving as metal binding sites confers good potential to obtain SCCOFs. More particularly, pre-synthesized COFs can be added to a solution of silver precursors, which can be reduced to produce silver nanoclusters within the COF network.

4.4 Multicomponent SCAMs

Borrowing ideas from biological systems like nucleic acids, lipids, proteins, *etc*. which are made of multiple building blocks, multicomponent SCAMs *i.e.* SCAMs composed of other metal clusters in addition to silver clusters or multiple kinds of linkers can bring in heterogeneity (complexity) without compromising structural order, thereby giving rise to unprecedented functional properties beyond the purview of regular SCAMs. Multicomponent SCAMs show great potential for photoluminescence sensing and cooperative catalysis owing to the synergistic influence of multiple components. However, the major challenge lies in suppressing the competing phases that can lead to other thermodynamically favorable single-component SCAMs as the main product rather than the desired multicomponent SCAMs. This can be accomplished by choosing suitable building units and effectively controlling the reaction conditions.

4.5 Cutting-edge applications

The rich plasmonic properties of silver clusters constituting SCAMs can be considered as a viable option for electronic communication applications.[77] Often, the uniformity of the surface or the distribution of the nanoparticles influences the material's performance. SCAMs could be crucial to preparing highly uniform materials with tunable properties. Regarding catalysis, more efficient and reusable SCAM-based catalysts are highly sought after. Optoelectronic device fabrication and integration techniques using SCAMs are imperative to practical applications.

The challenges and areas for improvement are briefly summarized in Fig. 6.

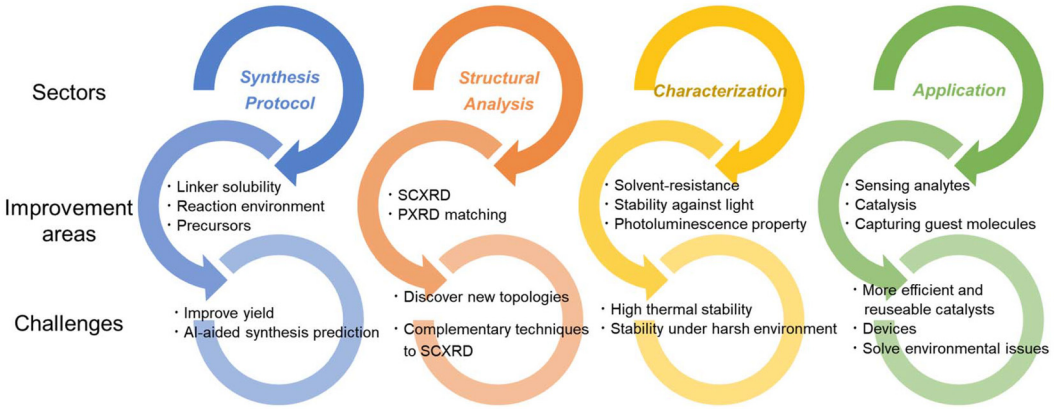

Fig. 6 Challenges and areas of improvement for SCAM research.

5. Final thoughts

Ever since their inception, SCAMs have been rapidly gaining momentum mainly driven by the flexible coordination nodes along with varying geometry and functionality of organic linker species to control framework connectivity. Hitherto, around 60 SCAMs have been reported and a significant portion of them display intense luminescence characteristics from electronic excited states and distinct luminescent responses to different analytes useful for selective sensing. SCAMs still have immense potential to accomplish exceptional optical properties when integrated into devices for leading-edge display and lighting technology, and intelligent switching and sensor platforms. Besides, chiral SCAMs are poised for significant impact in chiroptical detection systems.

Conflicts of interest

There are no conflicts to declare.

Acknowledgements

We acknowledge funding from the Japan Society for the Promotion of Science (JSPS) KAKENHI (grant no. 20H02698, 20H02552), the Scientific Research on Innovative Areas "Aquatic Functional Materials" (grant no. 22H04562), the Yazaki Memorial Foundation for Science and Technology, and the Ogasawara Foundation for the Promotion of Science and Engineering.

References

1 J. D. Aiken and R. G. Finke, *J. Mol. Catal. A: Chem.*, 1999, **145**, 1–44.
2 Y. Li, M. Zhou, Y. Song, T. Higaki, H. Wang and R. Jin, *Nature*, 2021, **594**, 380–384.
3 H. Qian, D.-e. Jiang, G. Li, C. Gayathri, A. Das, R. R. Gil and R. Jin, *J. Am. Chem. Soc.*, 2012, **134**, 16159–16162.
4 H. Zhang, T. Watanabe, M. Okumura, M. Haruta and N. Toshima, *Nat. Mater.*, 2012, **11**, 49–52.
5 Z. Lei, X.-K. Wan, S.-F. Yuan, Z.-J. Guan and Q.-M. Wang, *Acc. Chem. Res.*, 2018, **51**, 2465–2474.
6 A. W. Cook and T. W. Hayton, *Acc. Chem. Res.*, 2018, **51**, 2456–2464.
7 D. Li, B. Kumari, X. Zhang, C. Wang, X. Mei and V. M. Rotello, *Adv. Colloid Interface Sci.*, 2020, **276**, 102090.
8 Y. Akinaga, T. Kawawaki, H. Kameko, Y. Yamazaki, K. Yamazaki, Y. Nakayasu, K. Kato, Y. Tanaka, A. T. Hanindriyo, M. Takagi, T. Shimazaki, M. Tachikawa, A. Yamakata and Y. Negishi, *Adv. Funct. Mater.*, 2023, **33**, 2303321.
9 T. Kawawaki, Y. Mitomi, N. Nishi, R. Kurosaki, K. Oiwa, T. Tanaka, H. Hirase, S. Miyajima, Y. Niihori, D. J. Osborn, T. Koitaya, G. F. Metha, T. Yokoyama, K. Iida and Y. Negishi, *Nanoscale*, 2023, **15**, 7272–7279.
10 T. N. Gieshoff, U. Chakraborty, M. Villa and A. J. von Wangelin, *Angew. Chem., Int. Ed.*, 2017, **56**, 3585–3589.
11 J. N. Anker, W. P. Hall, O. Lyandres, N. C. Shah, J. Zhao and R. P. Van Duyne, *Nat. Mater.*, 2008, **7**, 442–453.
12 A. Desireddy, B. E. Conn, J. Guo, B. Yoon, R. N. Barnett, B. M. Monahan, K. Kirschbaum, W. P. Griffith, R. L. Whetten, U. Landman and T. P. Bigioni, *Nature*, 2013, **501**, 399–402.
13 R. Jin, C. Zeng, M. Zhou and Y. Chen, *Chem. Rev.*, 2016, **116**, 10346–10413.
14 W. Du, S. Jin, L. Xiong, M. Chen, J. Zhang, X. Zou, Y. Pei, S. Wang and M. Zhu, *J. Am. Chem. Soc.*, 2017, **139**, 1618–1624.
15 A. Ma, W. Du, J. Wang, K. Jiang, C. Zhang, W. Sheng, H. Zheng, R. Jin and S. Wang, *J. Phys. Chem. Lett.*, 2023, **14**, 5095–5101.
16 X. Wang, B. Yin, L. Jiang, C. Yang, Y. Liu, G. Zou, S. Chen and M. Zhu, *Science*, 2023, **381**, 784–790.
17 S. Biswas, S. Das and Y. Negishi, *Coord. Chem. Rev.*, 2023, **492**, 215255.

18 R.-W. Huang, Y.-S. Wei, X.-Y. Dong, X.-H. Wu, C.-X. Du, S.-Q. Zang and T. C. W. Mak, *Nat. Chem.*, 2017, **9**, 689–697.
19 R. Nakatani, S. Biswas, T. Irie, J. Sakai, D. Hirayama, T. Kawawaki, Y. Niihori, S. Das and Y. Negishi, *Nanoscale*, 2023, **15**, 16299–16306.
20 Z.-Y. Wang and S.-Q. Zang, in *Atomically Precise Nanochemistry*, 2023, pp. 479–501, DOI: 10.1002/9781119788676.ch16.
21 T. Sekine, J. Sakai, Y. Horita, H. Mabuchi, T. Irie, S. Hossain, T. Kawawaki, S. Das, S. Takahashi, S. Das and Y. Negishi, *Chem. – Eur. J.*, 2023, **29**, e202300706.
22 M. Cao, R. Pang, Q.-Y. Wang, Z. Han, Z.-Y. Wang, X.-Y. Dong, S.-F. Li, S.-Q. Zang and T. C. W. Mak, *J. Am. Chem. Soc.*, 2019, **141**, 14505–14509.
23 J.-Y. Wang, R.-W. Huang, Z. Wei, X.-J. Xi, X.-Y. Dong and S.-Q. Zang, *Chem. – Eur. J.*, 2019, **25**, 3376–3381.
24 X.-H. Wu, Z. Wei, B.-J. Yan, R.-W. Huang, Y.-Y. Liu, K. Li, S.-Q. Zang and T. C. W. Mak, *CCS Chem.*, 2019, **1**, 553–560.
25 M. Zhao, S. Huang, Q. Fu, W. Li, R. Guo, Q. Yao, F. Wang, P. Cui, C.-H. Tung and D. Sun, *Angew. Chem., Int. Ed.*, 2020, **59**, 20031–20036.
26 M. Cao, S. Wang, J.-H. Hu, B.-H. Lu, Q.-Y. Wang and S.-Q. Zang, *Adv. Sci.*, 2022, **9**, 2103721.
27 K. Zhou, C. Qin, X.-L. Wang, K.-Z. Shao, L.-K. Yan and Z.-M. Su, *CrystEngComm*, 2014, **16**, 7860–7864.
28 X. Wei, X. Kang, Z. Zuo, F. Song, S. Wang and M. Zhu, *Natl. Sci. Rev.*, 2021, **8**, nwaa077.
29 Z. Wang, X.-Y. Li, L.-W. Liu, S.-Q. Yu, Z.-Y. Feng, C.-H. Tung and D. Sun, *Chem. – Eur. J.*, 2016, **22**, 6830–6836.
30 Z.-Y. Chen, D. Y. S. Tam, L. L.-M. Zhang and T. C. W. Mak, *Chem. – Asian J.*, 2017, **12**, 2763–2769.
31 S. Chen, W. Du, C. Qin, D. Liu, L. Tang, Y. Liu, S. Wang and M. Zhu, *Angew. Chem., Int. Ed.*, 2020, **59**, 7542–7547.
32 R. Nakatani, S. Biswas, T. Irie, Y. Niihori, S. Das and Y. Negishi, *ACS Mater. Lett.*, 2024, **6**, 438–445.
33 J. Sakai, S. Biswas, T. Irie, H. Mabuchi, T. Sekine, Y. Niihori, S. Das and Y. Negishi, *Nanoscale*, 2023, **15**, 12227–12234.
34 Y.-H. Li, R.-W. Huang, P. Luo, M. Cao, H. Xu, S.-Q. Zang and T. C. W. Mak, *Sci. China: Chem.*, 2019, **62**, 331–335.
35 Z.-Y. Wang, M.-Q. Wang, Y.-L. Li, P. Luo, T.-T. Jia, R.-W. Huang, S.-Q. Zang and T. C. W. Mak, *J. Am. Chem. Soc.*, 2018, **140**, 1069–1076.
36 R.-W. Huang, X.-Y. Dong, B.-J. Yan, X.-S. Du, D.-H. Wei, S.-Q. Zang and T. C. W. Mak, *Angew. Chem., Int. Ed.*, 2018, **57**, 8560–8566.
37 M. J. Alhilaly, R.-W. Huang, R. Naphade, B. Alamer, M. N. Hedhili, A.-H. Emwas, P. Maity, J. Yin, A. Shkurenko, O. F. Mohammed, M. Eddaoudi and O. M. Bakr, *J. Am. Chem. Soc.*, 2019, **141**, 9585–9592.
38 Y.-M. Wang, J.-W. Zhang, Q.-Y. Wang, H.-Y. Li, X.-Y. Dong, S. Wang and S.-Q. Zang, *Chem. Commun.*, 2019, **55**, 14677–14680.
39 A. K. Das, S. Biswas, A. Thomas, S. Paul, A. S. Nair, B. Pathak, M. S. Singh and S. Mandal, *Mater. Chem. Front.*, 2021, **5**, 8380–8386.
40 N.-N. Li, M. Yang, X.-J. Xu, X.-Y. Dong, S. Li and S.-Q. Zang, *Dalton Trans.*, 2021, **50**, 15267–15273.
41 A. K. Das, S. Biswas, S. S. Manna, B. Pathak and S. Mandal, *Inorg. Chem.*, 2021, **60**, 18234–18241.
42 S. Biswas, A. K. Das, A. Nath, S. Paul, M. S. Singh and S. Mandal, *Nanoscale*, 2021, **13**, 17325–17330.
43 G. Deng, B. K. Teo and N. Zheng, *J. Am. Chem. Soc.*, 2021, **143**, 10214–10220.
44 Z. Wang, Y.-J. Zhu, Y.-Z. Li, G.-L. Zhuang, K.-P. Song, Z.-Y. Gao, J.-M. Dou, M. Kurmoo, C.-H. Tung and D. Sun, *Nat. Commun.*, 2022, **13**, 1802.
45 J.-Y. Wang, Y. Si, X.-M. Luo, Z.-Y. Wang, X.-Y. Dong, P. Luo, C. Zhang, C. Duan and S.-Q. Zang, *Adv. Sci.*, 2023, **10**, 2207660.
46 J.-Y. Wang, J.-W. Yuan, X.-M. Liu, Y.-J. Liu, F. Bai, X.-Y. Dong and S.-Q. Zang, *Aggregate*, 2024, e508.
47 X.-S. Du, B.-J. Yan, J.-Y. Wang, X.-J. Xi, Z.-Y. Wang and S.-Q. Zang, *Chem. Commun.*, 2018, **54**, 5361–5364.
48 M. Zhang, M. Cao, Z.-B. Sun, Z. Han, Z.-Y. Wang, Q.-Y. Wang and S.-Q. Zang, *Chem. Mater.*, 2023, **35**, 10238–10246.
49 Z. Wei, X.-H. Wu, P. Luo, J.-Y. Wang, K. Li and S.-Q. Zang, *Chem. – Eur. J.*, 2019, **25**, 2750–2756.
50 X.-H. Wu, P. Luo, Z. Wei, Y.-Y. Li, R.-W. Huang, X.-Y. Dong, K. Li, S.-Q. Zang and B. Z. Tang, *Adv. Sci.*, 2019, **6**, 1801304.
51 J.-Y. Wang, W.-H. Li, Z. Wei, C. Zhang, Y.-H. Li, X.-Y. Dong, G. Xu and S.-Q. Zang, *Chem. Commun.*, 2020, **56**, 2091–2094.
52 Q.-S. Wu, F. Bigdeli, F. Rouhani, X.-M. Gao, H. Kaviani, H.-J. Li, W. Wang, K.-G. Liu, M.-L. Hu, X.-Q. Cai and A. Morsali, *Inorg. Chem.*, 2021, **60**, 1523–1532.
53 J. Zhuge, F. Rouhani, F. Bigdeli, X.-M. Gao, H. Kaviani, H.-J. Li, W. Wang, M.-L. Hu, K.-G. Liu and A. Morsali, *Dalton Trans.*, 2021, **50**, 2606–2615.
54 C.-H. Gong, X.-Z. Hu, Z. Han, X.-F. Liu, M.-Z. Yang and S.-Q. Zang, *Chem. Commun.*, 2022, **58**, 1788–1791.
55 C.-H. Gong, Z.-B. Sun, M. Cao, X.-M. Luo, J. Wu, Q.-Y. Wang, S.-Q. Zang and T. C. W. Mak, *Chem. Commun.*, 2022, **58**, 9806–9809.
56 Z. Chang, X. Jing, C. He, X. Liu and C. Duan, *ACS Catal.*, 2018, **8**, 1384–1391.
57 Q.-X. Zang, Z.-Y. Wang, Y. Li, X.-M. Luo, H.-Y. Li, Y.-N. Si and S.-Q. Zang, *Chem. Commun.*, 2022, **58**, 11985–11988.
58 S.-R. He, H. Xu, C. Chen, X.-T. Wang, T.-Q. Lu, L. Cao, J. Zheng and X.-Y. Zheng, *Nanoscale*, 2023, **15**, 15730–15738.
59 X. Ma, C. Cai, W. Sun, W. Song, Y. Ma, X. Liu, G. Xie, S. Chen and S. Gao, *ACS Appl. Mater. Interfaces*, 2019, **11**, 9233–9238.
60 X.-Y. Dong, H.-L. Huang, J.-Y. Wang, H.-Y. Li and S.-Q. Zang, *Chem. Mater.*, 2018, **30**, 2160–2167.
61 X.-H. Ma, J.-Y. Wang, J.-J. Guo, Z.-Y. Wang and S.-Q. Zang, *Chin. J. Chem.*, 2019, **37**, 1120–1124.
62 X.-Y. Dong, Y. Si, J.-S. Yang, C. Zhang, Z. Han, P. Luo, Z.-Y. Wang, S.-Q. Zang and T. C. W. Mak, *Nat. Commun.*, 2020, **11**, 3678.

63 W. A. Dar, A. Jana, K. S. Sugi, G. Paramasivam, M. Bodiuzzaman, E. Khatun, A. Som, A. Mahendranath, A. Chakraborty and T. Pradeep, *Chem. Mater.*, 2022, **34**, 4703–4711.

64 K. Ghabili, P. S. Agutter, M. Ghanei, K. Ansarin and M. M. Shoja, *J. Appl. Toxicol.*, 2010, **30**, 627–643.

65 J. Kim, S.-N. Kim, H.-G. Jang, G. Seo and W.-S. Ahn, *Appl. Catal., A*, 2013, **453**, 175–180.

66 **https://www.who.int/news-room/fact-sheets/detail/antimicrobial-resistance#:~:text=It%20is%20estimated%20that%20bacterial,development%20of%20drug-resistant%.**

67 C. J. L. Murray, K. S. Ikuta, F. Sharara, L. Swetschinski, G. R. Aguilar, A. Gray, C. Han, C. Bisignano, P. Rao, E. Wool, S. C. Johnson, A. J. Browne, M. G. Chipeta, F. Fell, S. Hackett, G. Haines-Woodhouse, B. H. K. Hamadani, E. A. P. Kumaran, B. McManigal, S. Achalapong, R. Agarwal, S. Akech, S. Albertson, J. Amuasi, J. Andrews, A. Aravkin, E. Ashley, F.-X. Babin, F. Bailey, S. Baker, B. Basnyat, A. Bekker, R. Bender, J. A. Berkley, A. Bethou, J. Bielicki, S. Boonkasidecha, J. Bukosia, C. Carvalheiro, C. Castañeda-Orjuela, V. Chansamouth, S. Chaurasia, S. Chiurchiù, F. Chowdhury, R. C. Donatien, A. J. Cook, B. Cooper, T. R. Cressey, E. Criollo-Mora, M. Cunningham, S. Darboe, N. P. J. Day, M. D. Luca, K. Dokova, A. Dramowski, S. J. Dunachie, T. D. Bich, T. Eckmanns, D. Eibach, A. Emami, N. Feasey, N. Fisher-Pearson, K. Forrest, C. Garcia, D. Garrett, P. Gastmeier, A. Z. Giref, R. C. Greer, V. Gupta, S. Haller, A. Haselbeck, S. I. Hay, M. Holm, S. Hopkins, Y. Hsia, K. C. Iregbu, J. Jacobs, D. Jarovsky, F. Javanmardi, A. W. J. Jenney, M. Khorana, S. Khusuwan, N. Kissoon, E. Kobeissi, T. Kostyanev, F. Krapp, R. Krumkamp, A. Kumar, H. H. Kyu, C. Lim, K. Lim, D. Limmathurotsakul, M. J. Loftus, M. Lunn, J. Ma, A. Manoharan, F. Marks, J. May, M. Mayxay, N. Mturi, T. Munera-Huertas, P. Musicha, L. A. Musila, M. M. Mussi-Pinhata, R. N. Naidu, T. Nakamura, R. Nanavati, S. Nangia, P. Newton, C. Ngoun, A. Novotney, D. Nwakanma, C. W. Obiero, T. J. Ochoa, A. Olivas-Martinez, P. Olliaro, E. Ooko, E. Ortiz-Brizuela, P. Ounchanum, G. D. Pak, J. L. Paredes, A. Y. Peleg, C. Perrone, T. Phe, K. Phommasone, N. Plakkal, A. Ponce-de-Leon, M. Raad, T. Ramdin, S. Rattanavong, A. Riddell, T. Roberts, J. V. Robotham, A. Roca, V. D. Rosenthal, K. E. Rudd, N. Russell, H. S. Sader, W. Saengchan, J. Schnall, J. A. G. Scott, S. Seekaew, M. Sharland, M. Shivamallappa, J. Sifuentes-Osornio, A. J. Simpson, N. Steenkeste, A. J. Stewardson, T. Stoeva, N. Tasak, A. Thaiprakong, G. Thwaites, C. Tigoi, C. Turner, P. Turner, H. R. van Doorn, S. Velaphi, A. Vongpradith, M. Vongsouvath, H. Vu, T. Walsh, J. L. Walson, S. Waner, T. Wangrangsimakul, P. Wannapinij, T. Wozniak, T. E. M. W. Young-Sharma, K. C. Yu, P. Zheng, B. Sartorius, A. D. Lopez, A. Stergachis, C. Moore, C. Dolecek and M. Naghavi, *Lancet*, 2022, **399**, 629–655.

68 P. Beard, *Interface Focus*, 2011, **1**, 602–631.

69 Q. Fan, K. Cheng, Z. Yang, R. Zhang, M. Yang, X. Hu, X. Ma, L. Bu, X. Lu, X. Xiong, W. Huang, H. Zhao and Z. Cheng, *Adv. Mater.*, 2015, **27**, 843–847.

70 S. Xu, X. Shi, C. Chu and G. Liu, in *Methods Enzymol*, ed. J. Chan, Academic Press, 2021, vol. 657, pp. 145–156.

71 A. Thomas, S. Paul, J. Mitra and M. S. Singh, *Sensors*, 2021, **21**, 1190.

72 A. Star, E. Tu, J. Niemann, J.-C. P. Gabriel, C. S. Joiner and C. Valcke, *Proc. Natl. Acad. Sci. U. S. A.*, 2006, **103**, 921–926.

73 S. Das, T. Sekine, H. Mabuchi, S. Hossain, S. Das, S. Aoki, S. Takahashi and Y. Negishi, *Chem. Commun.*, 2023, **59**, 4000–4003.

74 C. E. Hughes, P. A. Williams and K. D. M. Harris, *Angew. Chem., Int. Ed.*, 2014, **53**, 8939–8943.

75 K. D. M. Harris, C. E. Hughes, P. A. Williams and G. R. Edwards-Gau, *Acta Crystallogr., Sect. C: Struct. Chem.*, 2017, **73**, 137–148.

76 C. G. Jones, M. W. Martynowycz, J. Hattne, T. J. Fulton, B. M. Stoltz, J. A. Rodriguez, H. M. Nelson and T. Gonen, *ACS Cent. Sci.*, 2018, **4**, 1587–1592.

77 A. S. Baburin, A. M. Merzlikin, A. V. Baryshev, I. A. Ryzhikov, Y. V. Panfilov and I. A. Rodionov, *Opt. Mater. Express*, 2019, **9**, 611–642.